International Journal of Solids and Structures 51 (2014) 2308–2326

Contents lists available at ScienceDirect

International Journal of Solids and Structures

journal homepage: www.elsevier.com/locate/ijsolstr

Analytical treatment of equilibrium configurations of cantilever under terminal loads using Jacobi elliptical functions

Milan Batista *

University of Ljubljana, Faculty of Maritime Studies and Transport, Pot pomorščakov 4, Portorož, EU, Slovenia

ARTICLE INFO

Article history:
Received 13 November 2013
Received in revised form 3 February 2014
Available online 25 March 2014

Keywords:
Elasticity
Cantilever
Exact solution
Elastica
Jacobi elliptical functions

ABSTRACT

The paper provides an exact analytical solution for the equilibrium configurations of a cantilever rod subject to inclined force and tip moment acting on its free end. The solution is given in terms of Jacobi's elliptical functions and illustrated by several numerical examples and several graphical presentations of shapes of deformed cantilevers. Possible forms of the underlying elastica of a cantilever are discussed in detail, and various simple formulas are given for calculating the characteristic dimensions of the elastica. For the case when a cantilever is subject only to applied force, three load conditions are discussed: the follower load problem, the load determination problem, and the conservative load problem. For all cases, either a formula or an effective procedure for determining the solution is provided. In particular, a new efficient procedure is given to determine all possible equilibrium shapes in the case of the conservative load problem.

1. Introduction

In this article, we discuss the problem of the determination of the deflection curve of an in-plane elastic cantilever rod subject to various forms of terminal force. The origin of the problem traces back to Galileo. In 1638, Galileo posed two problems concerning the construction of a cantilever. Over the following decades, these problems, through the works of Hook, Mariotte and Leibniz, gradually yielded to the question of determining the deflection curve of a cantilever. By 1691, James Bernoulli had narrowed this problem to the special case when terminal weight is acting on a column. The special case of terminal weight acting on a column was finally solved for the general case by Leonhard Euler in his famous treatise on elastic curves in 1743 (Euler, 1933) after a period of correspondence with Daniel Bernoulli. In his treatise, Euler enumerated nine possible equilibrium shapes for the infinite rod under equal but oppositely directed forces in a parametric study of the solution and then applied the classification to a cantilever. He found that a cantilever can be bent only into six shapes, considering only the non-inflection parts of an underlying elastic curve (elastica). The solution is presented in the form of two nonelementary integrals, using their power series expansions to make practical calculations. He also provided the formula for what we now call the critical force.

Upon the development of the theory of elliptic integrals and elliptic functions in the 19th century, researchers sought to obtain a closed form solution of the problem. One such solution was given by Clebsch (1862) (Section 53, pp 218–222), who considered a column under a vertical force but did not refer to elliptic integrals. In 1880, Saalschütz (1880) published a treatise that was entirely devoted to the determination of deflection curves of a cantilever under inclined force by using Legendre's elliptic integrals of the first and second types. In this book, we can find the closed-form expressions used to determine the shape of a deflected cantilever and special expressions for the displacement of its free end when the deflected cantilever is subjected to inclined, transversal or axial force. The closed-form solution in terms of Jacobi's elliptic functions was given in 1885 by Hess (1885) (Eqs. (18), (19)), who studied rods using Kirchhoff's kinetic analogy, which states that the equations pertaining to the elastic rod are equivalent to equations describing the motion of the rigid pendulum. Hess used Jacobi's notation of elliptic functions. The solution in Gudermann's notation was provided in 1893 by Love (1893) (Section 228 pp 49–54). Both of these solutions are, however, for the case of a rod under two oppositely directed forces and are not directly applicable to a cantilever. We note that Love called elastic curves with inflection points (corresponding to an oscillating pendulum) inflectional and the elastic curves without inflection points (corresponding to a revolving pendulum) noninflectional. Later editions of Love's book (Love, 1944) use his shortened version of the section about elastic lines. Born (1906), in his dissertation written in 1906, conducted

* Tel.: +386 5 6767 219.
E-mail address: milan.batista@fpp.uni-lj.si

http://dx.doi.org/10.1016/j.ijsolstr.2014.02.036
0020-7683/

the first experimental theoretical study of the post-buckling equilibrium configurations of a cantilever using an elliptic integral solution (for more historical data about the planar rod problems, we refer to Todhunter and Pearson (1960), Timoshenko (1953), Truesdell and Euler (1960), Goss (2003, 2009) and Levien (2008).

In the first half of the 20th century, numerous authors used or rediscovered Legendre's elliptic integral form for solving the cantilever problem. Malkin (1926) discussed large deformations of elastic columns under terminal weight. Hummel and Morton (1924) used the solution to implicitly measure Young's modulus of the cantilever rod. Barten (1944) provided an expression for the vertical deflection of the free end point of a cantilever loaded by transversal force, while Bisshopp and Drucker (1945), considering the same problem, also derived an expression for its free end axial displacement. Expressions for transversal and axial displacement of an axially loaded column can also be found in the work of Timoshenko and Gree (1961) (pp 76–82). In the 1948, the valuable book of Popov (1948) offered an extensive analysis of elastic rods using elliptic integrals. An updated and enlarged edition of the book (Popov, 1986) was published in the 1980s. Yet another derivation of an elliptic integral solution for the deflection of a cantilever under inclined force – using somewhat extensive notation – was given by Mitchell (1959).

Until the appearance of digital computers, the cantilever deflection was calculated using tables of elliptic integrals. Various approximate methods were proposed to overcome this difficulty. Beth and Wells (1951) provided a power series solution of the problem for an inclined force that is applicable for moderate cantilever deflection. Another power series solution for a transversally loaded cantilever, which results from a variant of the successive approximation method, was obtained by Scott et al. (1955). For inclined force, Frisch-Fay (1961, 1962) suggested a method by which a cantilever is broken into segments that are identical to a vertically loaded column and, in this way, replaced the integration with the solution of transcendental equations resulting from the condition of a smooth connection between the successive cantilever segments. The same author also published a valuable book treating flexible rods (Frisch-Fay, 1962), in which a chapter is devoted to the cantilever problem. Massoud (1966) considered a cantilever under transversal force and provided approximate formulas of deflection of the free end, derived by the selection of an axis with a slope that is the average value of the cantilever tangent angle. For references for the period up to the 1970s, we refer the reader to Schmidt and DaDeppo (1971).

The appearance of mainframe computers in the 1960s and 1970s allowed the use of various numerical techniques for solving the problems related to the cantilever. For this reason, the problem became the subject of many master's and doctoral theses; beyond this period, a further examination of relevant literature in a strict chronological manner is thus virtually impossible. We therefore omit a review of the articles that are closely related to the development of the finite element method (FEM) and cases in which the cantilever problem was used as a test example.

In 1981, Wang (1981) discussed the problem of deflection of an inclined cantilever subject to a vertical load. For a small and large value of applied force and for a nearly vertical cantilever under an arbitrarily valued force, he derived an approximate analytical expression using the perturbation method. For the general case, he used a numerical method. When one uses numerical methods, technically speaking, the cantilever problem is a two-point boundary value problem (BVP) in which one end has fixed geometric conditions and the other end has a prescribed load. Wang and later other authors therefore proposed a method that transforms the BVP into the initial value problem (IVP) that can be solved by direct numerical integration. Wang thus suggested a two-step method where, in each step, an initial value problem is solved using the Runge–Kutta numerical integration. In the first step, by selecting the value of the free end slope of the cantilever, Wang calculated the load parameter, the cantilever inclination and the bending moment at its clamped end. With these data, he then, in the next step, computed the cantilever deflection. Although Wang noted that his numerical method "is much easier than elliptic functions, which also require numerical evaluation," his method does not work if the initial data are the load parameter and cantilever inclination at the clamped end. Moreover, with the appearance of low-cost computers in the 1980s and the parallel development of numerical algorithms for calculating elliptic functions (Carlson and Notis, 1981), the elliptic integral solution became attractive for many researchers for various problems. Thus, Mattiasson (1981) published an article in which he provided tabular values of the displacement and the slant of a transversally loaded cantilever free end as a function of load parameter that can be used to check the results of numerical solutions against an exact solution. Lau (1982) provided closed-form solutions for a cantilever subject to an inclined force and tip moment in the form of elliptic integrals. The same load conditions were considered by DeBona and Zelenika (1997) in their article devoted to studying the limits of applying elliptic integral solutions in regard to the required degrees of calculation accuracy. Howell and Midha (1994) and Saxena and Kramer (1998) used the elliptic integral solution as part of a study of large deflections in compliant mechanisms, though the latter authors also included the free end bending moments among a cantilever load. Recently, Yau (2010) considered a guyed cantilever column pulled by an inclined cable (the problem already discussed by Saalschütz (1880) (Section 15)) and used the elliptic integral solution.

In 1992, Navaee (1992) published their famous article that considered a method for obtaining all possible equilibrium configurations of a cantilever beam under an inclined force. Their starting point was the well-known expression that results from the condition that a cantilever is inextensible and gives the load parameter as a function of the end slope in the form of a definite integral, i.e., the difference of two incomplete elliptic integrals of the first type. They observed that the upper and lower limits of the integral can have multiple values. Hence, for a given load parameter, the integral has multiple solutions for the end slope; in other words, these multiple solutions yield multiple possible equilibrium forms for a cantilever. Once Navaee and Elling numerically calculate the value of the end slope, they determine the coordinates of a deformed cantilever using the elliptic integral solution. They also consider the question of the number of possible equilibrium configurations but provide no general conclusion other than that the number of possible equilibrium configurations depends on the value of the load parameter and that the number can be odd or even. A drawback of their discussion is the lack of generality because they enumerate only seven possible equilibrium configurations; consequently, the graph illustrating the distribution of the load parameter versus the end slope is incomplete in that it fails to show that there is an infinite number of branches. The solution that they gave is thus applicable only to load parameters with values up to 12. In their next article, the authors established the possible range of end slope for a given force inclination (Navaee and Elling, 1993). A numerical procedure based on the Runge–Kutta integration that allows the determination of all equilibrium shapes of cantilever subject to inclined force was later provided by the present author (Batista and Kosel, 2005).

Until the beginning of the 1980s, researchers mainly considered the conservative load problem. The nonconservative problem (follower load problem) was considered by Popov (1948) and in connection with the stability of axially loaded columns (Pflüger, 1950; Bolotin, 1963). The solution for the cantilever subject to a nonconservative transversal force was given by Argyris and Syme-

onidis (1981) and Alliney and Tralli (1984) using FEM and, later, Saje and Srpcic (1985) (considering extensible beams), using the finite difference method. Recently, Shvartsman (2007) considered a nonuniform cantilever subjected to a tip-concentrated follower force by reducing the nonlinear two-point BVP to IVP following the transformation of the variable. As a result, the solution requires only one integration of the IVP. A similar method that transformed BVP to IVP by a reverse sense of integration was proposed by Nallathambi et al. (2010). The same problem was treated by Mutyalarao et al. (2010), who used a semianalytical approach. In this approach, the value of the cantilever free end slope serves as input data, with which the load parameter is calculated and expressed as an elliptic integral. With these data, the problem becomes an IVP that can then be solved using the Runge–Kutta numerical integration. Recently, Karlson and Leamy (2013) used the cantilever follower load problem to validate their shooting method treatment.

Several articles published by a group of Russian researchers at the beginning of this century deserve special attention. Zakharov and Zakharenko (1999) considered the dynamic instability of a cantilever under a transversal force, viewing it as an eigenvalue problem where the characteristic equation was obtained from the condition that the bending moment vanishes at the free end. They expressed their solution using Jacobi's elliptic functions. For each eigenvalue, there is a characteristic critical force, which consequently yields a different number of deflected cantilever inflection points. According to Zakharov and Zakharenko, cantilever deflection without inflection points is static, and cantilever deflection with inflection points is dynamic. A similar solution for an inclined force was given by Zakharov and Okhotkin (2002) and for a nonconservative inclined force by Zakharov et al. (2004). Kuznetsov and Levyakov (2002) and Levyakov and Kuznetsov (2010) examined the stability of the post-buckling equilibrium states of rods (including cantilevers) and used Jacobi elliptic function solution in their discussion.

Some semianalytical methods were recently proposed for solving the cantilever problem. Wang et al. (2008) provided a solution for the case of a transverse conservative force using the homotopy method, which expresses an explicit approximate solution of the problem in the form of a truncated arc-length parameter power series wherein the series coefficients are calculated numerically. Using the same method, Kimiaeifar and et al. (2011) offered a solution of the problem for a nonconservative inclined force and bending moment, and Wang et al. (2012) considered a cantilever under inclined follower force using transformation of the variable from Shvartsman (2007). The deflected cantilevers displayed in these articles do not include inflection points. Tari (2013) solved the problem using what he calls the automatic Taylor expansion technique. In essence, he approximated the solution by expanding unknowns as a power series of an arc-length parameter. He presented his solutions in graphical form, but again, none of the displayed deflected cantilevers subject only to tip force included inflection points.

We note that numerous articles address the cantilever subject with a more complex load and possibly include geometric and/or material nonlinearities (Banerjee et al., 2008). Numerous articles also treat the stability of elastica equilibrium forms (Maddocks, 1984; Sachkov and Levyakov, 2010) and the application of elastica theory in computer graphics (Linner, 1998), DNA modeling (Coleman and Swigon, 2000), and hair modeling (Audoly and Pomeau, 2010). However, because these works are not directly related to the present problem, they were not considered.

The aim of this paper is to give yet another analytical solution for the cantilever problem, where we treat its possible load conditions from a single point of view. From the review, we see that there are in essence three analytical approaches to the problem: using Legendre elliptic integrals, where the independent variable is the cantilever tangent angle; using Jacobi elliptical functions, where the independent parameter is the cantilever arc length; and various series expansions. The first two methods are clearly superior because they obtain a closed-form solution that includes all possible cantilever equilibrium configurations. In our opinion, the Jacobi elliptical functions are more flexible for a discussion of the problem as elliptic integrals. Therefore, we use Jacobi's elliptic functions in the solution of the problem.

In the organization of the article, we first give the derivation of the basic equations where we, apart from slightly changed notation, follow Antman (1995) (Chapter IV). The next two sections are devoted to the solution of the basic equations, and the fifth section gives some numerical values and some comparison with results of other authors. In the sixth section, we discuss possible shapes of cantilevers underlying elastic in detail, and in the seventh section, we apply the solution to discuss various force load conditions. The article ends with a summary of the obtained results.

2. Formulation of the problem

2.1. Geometry and equilibrium

We consider an initially straight inextensible and unshearable elastic rod of length L, with one end clamped and a force and tip bending moment acting at the other end. In the Cartesian coordinate system Oxy, the shape of the deformed base curve of the cantilever is described using the following differential equations (Antman, 1995, pp 87–88):

$$\frac{dx}{ds} = -\cos\phi, \quad \frac{dy}{ds} = -\sin\phi \tag{1}$$

$$\frac{d\phi}{ds} = -\kappa \tag{2}$$

where $x(s)$ and $y(s)$ are coordinates of the base curve, $\phi(s)$ is the angle between the tangent to the base curve and the x-axis, $\kappa(s)$ is the base curve curvature and $s \in [0, L]$ is the arc length parameter measured from the cantilever free end to the cantilever clamped end (Fig. 1).

The equilibrium equations of the cantilever are (Antman, 1995, p. 96)

$$H = -F\cos\gamma, \quad V = F\sin\gamma \tag{3}$$

$$\frac{dM}{ds} = -H\sin\phi + V\cos\phi = F\sin(\phi+\gamma) \tag{4}$$

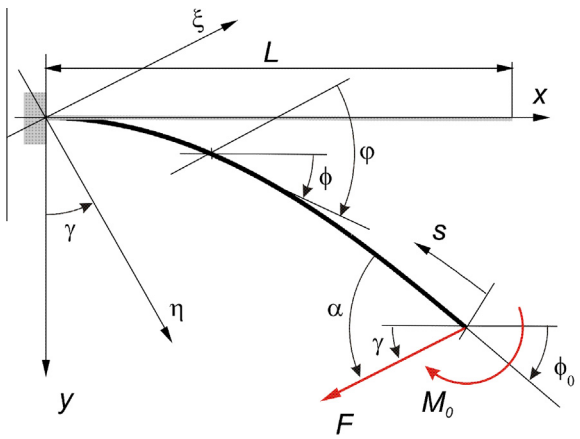

Fig. 1. Geometry and load of the problem.

where H and V are the horizontal and the vertical components of the internal force, $M(s)$ is the bending moment, $F \geqslant 0$ is the magnitude of the terminal force and γ is the angle between the x-axis and the direction of force. If α is the angle between the tangent to the cantilever base curve at the free point and the direction of the terminal force and ϕ_0 is the free end tangent angle, then

$$\gamma = \alpha - \phi_0, \quad \phi_0 \equiv \phi(0) \tag{5}$$

We assume that the moment and the curvature are related by the Bernoulli–Euler constitutive equation:

$$M = EI\kappa \tag{6}$$

where EI is assumed to be a positive constant that represents the flexural rigidity of the cantilever. This equation together with the system of differential Eqs. (1), (2), and (4) constitutes a complete set of equations for the unknowns $x(s)$, $y(s)$, $\phi(s)$, $\kappa(s)$ and $M(s)$. The task is to solve these equations subject to the following boundary conditions

$$x(L) = y(L) = 0, \quad \phi(L) = 0 \quad \text{(clamped end)} \tag{7}$$

$$M(0) = M_0 \quad \text{(free end)} \tag{8}$$

where M_0 is the applied moment.

2.2. Nondimensional form of equations

The equation of the problem contains five parameters: F, M_0, EI, L and γ. We reduce this number by introducing the load parameter ω, which is defined by

$$\omega^2 \equiv \frac{FL^2}{EI} \tag{9}$$

the dimensionless curvature of the cantilever free end κ_0, which is defined by

$$\kappa_0 \equiv \frac{M_0 L}{EI} \tag{10}$$

and the following normalization of the geometric variables:

$$\frac{s}{L} \to s \in [0,1], \quad \frac{x(s)}{L} \to x(s), \quad \frac{y(s)}{L} \to y(s), \quad L\kappa(s) \to \kappa(s) \tag{11}$$

We obtain some future simplification of the equations by introducing a new local coordinate system $O\xi\eta$ that is, with respect to coordinate system Oxy, rotated by the angle $-\gamma$ so that the line of action of the applied force becomes parallel to the ξ axis (Fig. 1). In the new coordinate system, the coordinates $\xi(s)$ and $\eta(s)$ of the cantilever base curve are

$$\xi(s) = x(s)\cos\gamma - y(s)\sin\gamma, \quad \eta(s) = x(s)\sin\gamma + y(s)\cos\gamma \tag{12}$$

and the angle $\varphi(s)$ between the tangent to the cantilever base curve and the ξ-axis is

$$\varphi(s) = \phi(s) + \gamma \tag{13}$$

The differential equations that describe the cantilever shape in $O\xi\eta$ are obtained by differentiating (12) with respect to s and then using (1) and (13). This process yields

$$\frac{d\xi}{ds} = -\cos\varphi, \quad \frac{d\eta}{ds} = -\sin\varphi \tag{14}$$

and from $(7)_{1,2}$ and (12), the associated boundary conditions are

$$\xi(1) = 0, \quad \eta(1) = 0 \tag{15}$$

Using (6), (9), and (13), the differential equations (2) and (4) become

$$\frac{d\varphi}{ds} = -\kappa, \quad \frac{d\kappa}{ds} = \omega^2 \sin\varphi \tag{16}$$

and from $(7)_3$ and (8), the associated boundary conditions are

$$\varphi(0) = \alpha, \quad \kappa(0) = \kappa_0 \tag{17}$$

Using a selected sense of integration and rotation of the coordinate system, we thus transform the original two-point boundary value problem into a three-parameter initial value problem given by Eqs. (16) and (17) for the unknowns $\varphi = \hat{\varphi}(s;\alpha,\omega,\kappa_0)$ and $\kappa = \hat{\kappa}(s;\alpha,\omega,\kappa_0)$. Once these functions have been determined, we can obtain the coordinates of a deformed cantilever base curve $\xi = \hat{\xi}(s;\alpha,\omega,\kappa_0)$ and $\eta = \hat{\eta}(s;\alpha,\omega,\kappa_0)$ through the integration of Eq. (14), subject to the boundary conditions found in Eq. (15). Further, from Eq. (13), the tangent angle ϕ is

$$\phi(s) = \varphi(s) - \gamma \tag{18}$$

and by solving Eq. (12) for $x(s)$ and $y(s)$, we finally obtain

$$x(s) = \xi(s)\cos\gamma + \eta(s)\sin\gamma, \quad y(s) = -\xi(s)\sin\gamma + \eta(s)\cos\gamma \tag{19}$$

Because the right-hand sides of Eqs. (16) and (14) are continuous functions, the existence theorem for ordinary differential equations guarantees the uniqueness of the solution for the given initial conditions (Hirsch et al., 2004, pp 144).

We see that the shape of a deformed cantilever depends on the parameters α, ω and κ_0 and that its spatial position depends on γ. The relationship among α, ω, κ_0 and γ is obtained from Eq. (18). When $s = 1$, we must have $\phi(1) = 0$, and therefore, by Eq. (18),

$$\gamma = \hat{\varphi}(1;\alpha,\omega,\kappa_0) = \hat{\gamma}(\alpha,\omega,\kappa_0) \tag{20}$$

This relationship is fundamental, allowing us to define various types of problems. Some of the problems are discussed in Section 7. Until then, we assume that the given parameters are α, ω, and κ_0.

2.3. Symmetry

If, in the initial conditions of Eq. (17), we replace α with $-\alpha$ and κ_0 with $-\kappa_0$, then Eqs. (14), (16), (18), and (19) imply the following symmetry

$$\begin{aligned}
&\kappa(s;-\alpha,-\kappa_0) = -\kappa(s;\alpha,\kappa_0), \quad \varphi(s;-\alpha,-\kappa_0) = -\varphi(s;\alpha,\kappa_0)\\
&\xi(s;-\alpha,-\kappa_0) = \xi(s;\alpha,\kappa_0), \quad \eta(s;-\alpha,-\kappa_0) = -\eta(s;\alpha,\kappa_0)\\
&\phi(s;-\alpha,-\kappa_0) = -\phi(s;\alpha,\kappa_0), \quad x(s;-\alpha,-\kappa_0) = x(s;\alpha,\kappa_0),\\
&y(s;-\alpha,-\kappa_0) = -y(s;\alpha,\kappa_0)
\end{aligned} \tag{21}$$

The equations in (21) show that the functions $\kappa(s)$, $\varphi(s)$, $\phi(s)$, $\eta(s)$ and $y(s)$ are odd and that $\xi(s)$ and $x(s)$ are even functions of α and κ_0. The deformed shape of cantilever is thus symmetric with respect to the ξ -axis and the x-axis when α and κ_0 change sign.

3. Two special solutions

3.1. Trivial solution

The initial value problem (16) and (17) has the following trivial solution (Antman, 1995, pp 217). When $\kappa_0 = 0$, the boundary conditions shown in Eq. (17) are satisfied by

$$\varphi(s) = \alpha \quad \text{and} \quad \kappa(s) = 0 \tag{22}$$

From Eq. (20), we then obtain $\gamma = \alpha$, while the system shown in Eq. (16) is reduced to $\sin\alpha = 0$, so we must have $\alpha = \pm n\pi$, where n is any integer, yielding two physical possibilities:

1. $\alpha = \gamma = 0$ (pure compression) or
2. $\alpha = \gamma = \pm\pi$ (pure extension).

In either case, from Eq. (13), we obtain $\phi(s) = 0$. Therefore, the equations for cantilever shape shown in (1) are reduced to $\frac{dx}{ds} = -1$ and $\frac{dy}{ds} = 0$; after integration under the boundary conditions in (15), these yield

$$x(s) = 1 - s \quad \text{and} \quad y(s) = 0$$

For the trivial solution, the cantilever under arbitrary force remains straight. In the future, because the solution of an initial value problem is unique, we conclude that in the cases when $\alpha = 0$ or when $\alpha = \pm\pi$, the only possible solution to the problem is the trivial solution.

3.2. Cantilever subject only to tip moment

In this case, $\omega = 0$ and $\gamma = 0$, so by Eq. (18), we have $\phi(s) = \varphi(s)$, while Eq. (16) is reduced to

$$\frac{d\varphi}{ds} = -\kappa, \quad \frac{d\kappa}{ds} = 0 \tag{23}$$

The integration of these equations under the boundary conditions of Eq. (17) and the condition $\varphi(1) = 0$ yields

$$\varphi = \kappa_0(1 - s), \quad \kappa = \kappa_0 \tag{24}$$

where $\alpha = \kappa_0$. From Eqs. (14), (15), and (19), we then have

$$x = \frac{\sin(\kappa_0(1-s))}{\kappa_0}, \quad y = \frac{1 - \cos(\kappa_0(1-s))}{\kappa_0} \tag{25}$$

This result is well known and shows that a cantilever deforms into a circular arc lying on the circle:

$$x^2 + \left(\frac{1}{\kappa_0} - y\right)^2 = 1/\kappa_0^2. \tag{26}$$

From Eq. (25), the coordinates of the cantilever free end are

$$x_0 \equiv x(0) = \frac{\sin\kappa_0}{\kappa_0}, \quad y_0 \equiv y(0) = \frac{1 - \cos\kappa_0}{\kappa_0}. \tag{27}$$

In the special case when $x_0 = 0$, we have $\kappa_0 = n\pi$, $(n = \pm1, \pm2, \ldots)$ and $y_0 \equiv y(0) = \frac{1-(-1)^n}{n\pi}$ from Eq. (27). The underlying circle in this case is $x^2 + (1/n\pi - y)^2 = 1/(n\pi)^2$. The cantilever deforms to n overlapping circles when n is even; i.e., when $\kappa_0 = 2m\pi$, $(m = 1, 2, \ldots)$. When $n \to \infty$, the cantilever reduces to a point.

Hereafter, we assume that $\omega > 0$.

4. General solution

The procedure for the solution of the initial value problem of Eqs. (16) and (17) is well known Greenhill, 1892; Armitage et al., 2006, and we here, for completeness, reproduce only the essential steps. In first step, by the standard transformation $\frac{d\kappa}{ds} = \frac{d\kappa}{d\varphi}\frac{d\varphi}{ds} = \frac{d}{d\varphi}\left(\frac{\kappa^2}{2}\right)$ and integration under the boundary conditions of Eq. (17), we obtain the first integral:

$$\frac{d\varphi}{ds} = \sqrt{2\omega^2(\cos\varphi - \cos\alpha) + \kappa_0^2} = 2\omega\sqrt{\sin^2\frac{\alpha}{2} - \sin^2\frac{\varphi}{2} + \left(\frac{\kappa_0}{2\omega}\right)^2} \tag{28}$$

We now discuss several cases of the solution of this equation.

4.1. Force dominant case

In the force dominant case, $\sin^2\frac{\alpha}{2} + \left(\frac{\kappa_0}{2\omega}\right)^2 < 1$. By introducing a new variable $\psi(s)$ defined by

$$\sin\frac{\varphi}{2} = k\sin\psi \tag{29}$$

where k is the modulus defined by

$$k \equiv \sqrt{\sin^2\frac{\alpha}{2} + \left(\frac{\kappa_0}{2\omega}\right)^2} \tag{30}$$

we transform Eq. (28) into the following form

$$\frac{d\psi}{\omega\, ds} = \sqrt{1 - k^2\sin^2\psi} \tag{31}$$

If we further set

$$u \equiv \sin\psi \tag{32}$$

then Eq. (31) takes the Jacobi normal form

$$\frac{du}{\omega\, ds} = \sqrt{1-u^2}\sqrt{1-k^2u^2} \tag{33}$$

The general solution of this equation is

$$u(s) = \mathrm{sn}(\omega s + C, k) \tag{34}$$

where C is the constant of integration and sn is the Jacobi elliptic sine function. Using Eqs. (32), (29), and $(16)_1$, we find the solution of the problem (see also Zakharov and Okhotkin, 2002; Zakharov et al., 2004)

$$\varphi(s) = 2\sin^{-1}[k\,\mathrm{sn}(\omega s + C, k)] \tag{35}$$

$$\kappa(s) = -2\omega k\,\mathrm{cn}(\omega s + C, k) \tag{36}$$

where cn is Jacobi's elliptic cosine function. When $s = 1$, Eq. (35) yields the explicit expression for Eq. (20).

$$\gamma = 2\sin^{-1}[k\,\mathrm{sn}(\omega + C, k)] \tag{37}$$

The graph of this function for the special case when $\kappa_0 = 5$ is shown in Fig. 2(b).

The constant of integration C is determined from the initial conditions shown in Eq. (17). By equating these conditions with the values of Eqs. (35) and (36) for $s = 0$, we obtain two equations

$$\mathrm{sn}(C, k) = \frac{\sin(\alpha/2)}{k} - 2\omega k\,\mathrm{cn}(C, k) = \kappa_0 \tag{38}$$

Inspecting the four possible combinations of signs of α and κ_0 yields the following expression for C:

$$C = \begin{cases} \mathrm{sn}^{-1}\left(\frac{\sin(\alpha/2)}{k}, k\right) & \kappa_0 < 0 \\ 2K - \mathrm{sn}^{-1}\left(\frac{\sin(\alpha/2)}{k}, k\right) & \kappa_0 > 0 \end{cases} \tag{39}$$

where $K = K(k)$ is a complete elliptic integral of the first type.

Now, to integrate Eq. (14) using Eq. (35), we first express

$$\begin{aligned} \cos\varphi &= 1 - 2\sin^2\frac{\varphi}{2} = 1 - 2k^2\mathrm{sn}^2(\omega s + C, k) = -1 + 2\mathrm{dn}^2(\omega s + C, k) \\ \sin\varphi &= 2\sin\frac{\varphi}{2}\cos\frac{\varphi}{2} = 2\mathrm{sn}(\omega s + C, k)\sqrt{1 - k^2\mathrm{sn}^2(\omega s + C, k)} \\ &= 2k\,\mathrm{sn}(\omega s + C, k)\mathrm{dn}(\omega s + C, k) \end{aligned} \tag{40}$$

where dn is the Jacobi elliptic delta function. The integral of these functions is (Armitage et al., 2006):

$$\begin{aligned} \int \cos\varphi\, ds &= -s + \frac{2}{\omega}\int \mathrm{dn}^2(z + C, k)\, dz = -s + \frac{2}{\omega}\varepsilon(\omega s + C, k) \\ \int \sin\varphi\, ds &= \frac{2}{\omega}\int \mathrm{sn}(z + C, k)\mathrm{dn}(z + C, k)\, dz = -\frac{2}{\omega}\mathrm{cn}(\omega s + C, k) \end{aligned} \tag{41}$$

where ε is Jacobi's epsilon function (Olver et al., 2010, 22.16.17, p. 562, Whittaker et al., 1927, p. 517)

$$\varepsilon(z, k) \equiv \int_0^z \mathrm{dn}^2(t, k)\, dt \tag{42}$$

Instead of the Jacobi epsilon function, we use the Jacobi zeta function that is defined as (Olver et al., 2010, 22.16.32, p. 562)

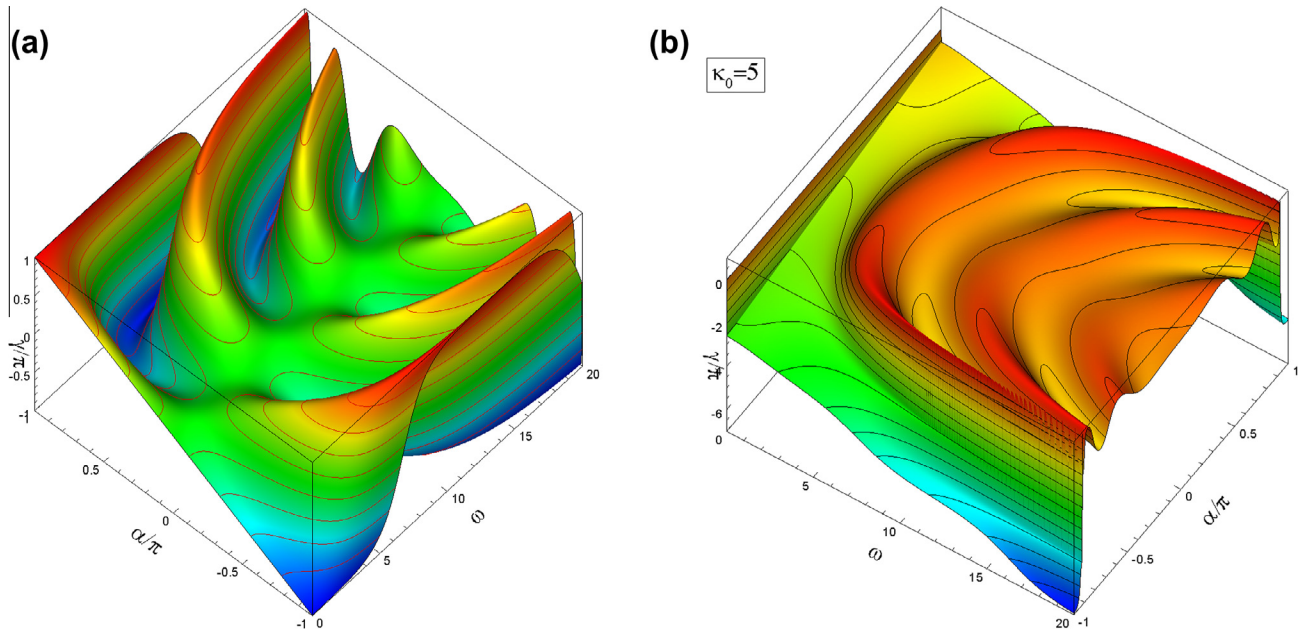

Fig. 2. On the left is (a) the graph of $\gamma = \hat{\gamma}(\alpha, \omega, \kappa_0)$ given by Eq. (37) when $\kappa_0 = 5$. On the right is (b) the graph of $\gamma = \hat{\gamma}(\alpha, \omega)$ given by Eq. (70). Note that at the end of interval, $\gamma(\omega, \pm\pi) = \pm\pi$ (not displayed).

$$Z(z,k) \equiv \varepsilon(z,k) - \frac{E}{K}z \tag{43}$$

where E is a complete Legendre elliptic integral of the second type. Introducing the Jacobi zeta function has several advantages. First, introducing the Jacobi zeta function clearly separates the periodic part of the solution from its nonperiodic part. Second, the periodic part becomes bounded. Third, the Jacobi zeta function is part of the Maple program, while the Jacobi epsilon function is not.

By substituting Eq. (41) into Eq. (14) and then applying the boundary conditions shown in Eq. (15), we obtain the following parametric equations of a deformed cantilever base curve in the local coordinate system.

$$\begin{aligned}\xi(s) &= \left(\frac{2E}{K} - 1\right)(1-s) + \frac{2}{\omega}[Z(\omega + C, k) - Z(\omega s + C, k)] \\ \eta(s) &= -\frac{2k}{\omega}[\mathrm{cn}(\omega + C, k) - \mathrm{cn}(\omega s + C, k)]\end{aligned} \tag{44}$$

Before proceeding, we derive some inequalities based on the fact that the trigonometric and Jacobian elliptic functions oscillate between -1 and 1. Assume that $\alpha \geqslant 0$. Then, from Eq. (35), we obtain the interval for the tangent angle

$$|\varphi(s)| \leqslant \alpha \tag{45}$$

Here, we consider that α is physically bounded to interval $[-\pi, \pi]$, and so in Eq. (35), we must take the principal value of function $\sin^{-1}$. In this way, the expression shown in Eq. (37) gives the unique value of γ. In particular, for $s = 0$, we obtain (see also Zakharov et al., 2004, Eq. (11))

$$|\gamma| \leqslant \alpha \tag{46}$$

From this inequality and Eq. (5), the range for the free end tangent angle is as follows (see also Navaee and Elling, 1993):

$$0 \leqslant \phi_0 \leqslant 2\alpha \tag{47}$$

The range for a cantilever curvature follows from Eq. (36) and is

$$|\kappa(s)| \leqslant 2\omega. \tag{48}$$

4.2. Moment dominant case

In the moment dominant case, $\sin^2\frac{\alpha}{2} + \left(\frac{\kappa_0}{2\omega}\right)^2 \geqslant 1$. By setting $\psi = \phi/2$ from Eq. (28), we obtain the following equation:

$$\frac{d\psi}{\omega\, ds} = k\sqrt{1 - k^{-2}\sin^2\psi} \tag{49}$$

which, after performing similar transformations as in the previous case, leads to the solution of Eq. (16) in the form

$$\varphi(s) = -2\mathrm{sgn}(\kappa_0)\ \mathrm{am}(k\omega s + C, k^{-1}) \tag{50}$$

$$\kappa(s) = 2\mathrm{sgn}(\kappa_0)\omega k\,\mathrm{dn}(k\omega s + C, k^{-1}) \tag{51}$$

where $\mathrm{am}(x) = \arcsin(\mathrm{sn}(x))$ is Jacobi's amplitude function and constant C is given by

$$C = -\mathrm{sgn}(\kappa_0)\mathrm{sn}^{-1}\left(\sin\frac{\alpha}{2}, k^{-1}\right) \tag{52}$$

The choices of signs in these equations deserve an explanation. Because dn is always positive, the sign of κ is determined from the initial conditions. Now assume that $\kappa_0 > 0$. According to Eq. $(16)_1$, the derivation of φ should be negative, therefore Eq. (50) must be a negative signet. However, for $\alpha > 0$, we must have $\varphi(0) = -2\mathrm{am}(C, k^{-1}) > 0$, and C should therefore be negative. The reasoning for $\kappa_0 < 0$ is similar. The explicit form of Eq. (20) is in this case from Eq. (50)

$$\gamma = -2\mathrm{sgn}(\kappa_0)\mathrm{am}(k\omega + C, k^{-1}) \tag{53}$$

To integrate Eq. (14), we first note that $\cos\mathrm{am}(x) = \mathrm{cn}x$ and $\sin\mathrm{am}(x) = \mathrm{sn}x$. Hence, using Eq. (50), we obtain

$$\begin{aligned}\cos\varphi &= 1 - 2\,\mathrm{sn}^2(k\omega s + C, k^{-1}) = 1 - 2k^2 - 2k^2\mathrm{dn}^2(k\omega s + C, k^{-1}) \\ \sin\varphi &= -2\mathrm{sgn}(\kappa_0)\,\mathrm{sn}(k\omega s + C, k^{-1})\mathrm{cn}(k\omega s + C, k^{-1})\end{aligned} \tag{54}$$

and therefore

$$\begin{aligned}\int \cos\varphi\, ds &= s - \frac{2}{k\omega}\int \mathrm{sn}^2(z+C,k^{-1})\,dz \\ &= (1-2k^2)s + \frac{2k}{\omega}\varepsilon(k\omega s + C, k^{-1}) \\ \int \sin\varphi\, ds &= -\frac{2\,\mathrm{sgn}(\kappa_0)}{\omega k}\int \mathrm{sn}(z+C,k^{-1})\,\mathrm{cn}(z+C,k^{-1})\,dz \\ &= \mathrm{sgn}(\kappa_0)\frac{2k}{\omega}\,\mathrm{dn}(k\omega s + C, k^{-1})\end{aligned} \tag{55}$$

Using the above integrals under the conditions shown in Eq. (15), from Eq. (14), we obtain the parametric equation of a cantilever base curve in the form

$$\begin{aligned}\xi(s) &= \left[2k^2\left(\frac{E(k^{-1})}{K(k^{-1})}-1\right)+1\right](1-s)+\frac{2k}{\omega}[Z(k\omega+C,k^{-1})-Z(k\omega s+C,k^{-1})] \\ \eta(s) &= \mathrm{sgn}(\kappa_0)\frac{2k}{\omega}[\mathrm{dn}(k\omega+C,k^{-1})-\mathrm{dn}(k\omega s+C,k^{-1})]\end{aligned} \tag{56}$$

Consider now the special case when $\kappa_0/\omega \to \infty$ and therefore $k^{-1} \to 0$. Using the Maclaurin series of functions dn (Olver et al., 2010, 22.10.6, p. 559) and the definition shown in Eq. (43), we obtain the following expansion of Z with respect to k

$$Z(z,k) = -\left(1-\frac{E(k)}{K(k)}\right)z - \frac{k^2}{4}(2z-\sin 2z) + O(k^4) \tag{57}$$

Further, we have

$$\lim_{k\to\infty} 2k^2\left(\frac{E(1/k)}{K(1/k)}-1\right) = -1 \tag{58}$$

From Eqs. (50), (51), and (56), we can now deduce

$$\varphi(s) \to -\kappa_0 s + \alpha, \quad \kappa(s) \to \kappa_0 \tag{59}$$

$$\begin{aligned}\xi(s) &\to \frac{\sin(\kappa_0-\alpha)-\sin(\kappa_0 s-\alpha)}{\kappa_0} \\ \eta(s) &\to \frac{\cos(\kappa_0-\alpha)-\cos(\kappa_0 s-\alpha)}{\kappa_0}\end{aligned} \tag{60}$$

and from Eqs. (18) and (19)

$$\phi(s) \to \kappa_0(1-s)$$

$$x(s) \to \frac{\sin[\kappa_0(1-s)]}{\kappa_0}, \quad y(s) \to \frac{1-\cos[\kappa_0(1-s)]}{\kappa_0} \tag{61}$$

These equations show that the solution approaches the solution of a cantilever subject only to a tip moment.

4.3. Case when $k = 1$

The condition in case $\alpha = \pi$ implies $\kappa_0 = 0$, and this case is covered by a trivial solution. For $|\alpha| < \pi$, from Eq. (30), we have

$$\kappa_0 = 2\omega\cos\frac{\alpha}{2} \tag{62}$$

where we assume that $\kappa_0 > 0$. From Eqs. (50), (51), (53), and (56), we then obtain

$$\varphi(s) = -2\sin^{-1}[\tanh(\omega s + C)], \quad \kappa(s) = \frac{2\omega}{\cosh(\omega s + C)} \tag{63}$$

$$\begin{aligned}\xi(s) &= -1 + s + \frac{2}{\omega}[\tanh(\omega + C) - \tanh(\omega s + C)] \\ \eta(s) &= \frac{2}{\omega}\left[\frac{1}{\cosh(\omega + C)} - \frac{1}{\cosh(\omega s + C)}\right]\end{aligned} \tag{64}$$

where, from Eq. (52),

$$C = -\tanh^{-1}\left(\sin\frac{\alpha}{2}\right) \tag{65}$$

4.4. Case when $\kappa_0 = 0$

In this special case, from Eq. (30), we have

$$k \equiv \sin\frac{\alpha}{2} \tag{66}$$

and Eq. (39) therefore becomes

$$C = \mathrm{sn}^{-1}(1) = K(k) \tag{67}$$

From Eqs. (35) and (36), we have

$$\varphi(s) = 2\sin^{-1}[k\,\mathrm{sn}(\omega s + K, k)] = 2\sin^{-1}\left[k\frac{\mathrm{cn}(\omega s,k)}{\mathrm{dn}(\omega s,k)}\right] \tag{68}$$

$$\kappa(s) = -2\omega k\,\mathrm{cn}(\omega s + K, k) = 2\omega k k'\frac{\mathrm{sn}(\omega s,k)}{\mathrm{dn}(\omega s,k)} \tag{69}$$

where $k' = \sqrt{1-k^2}$. In particular, from Eq. (68) for $s = 1$, we obtain

$$\gamma = 2\sin^{-1}[k\,\mathrm{sn}(\omega + K, k)] = 2\sin^{-1}\left[k\frac{\mathrm{cn}(\omega,k)}{\mathrm{dn}(\omega,k)}\right] \tag{70}$$

The graph of this function is shown in Fig. 2(a). The parametric equations for a deformed cantilever shape in a local coordinate system follow from Eq. (44) and are

$$\begin{aligned}\xi(s) &= \left(\frac{2E}{K}-1\right)(1-s)+\frac{2}{\omega}[Z(\omega+K,k)-Z(\omega s+K,k)] \\ &= \left(\frac{2E}{K}-1\right)(1-s)+\frac{2}{\omega}\{Z(\omega,k)-Z(\omega s,k) \\ &\quad -k^2\left[\frac{\mathrm{sn}(\omega,k)\mathrm{cn}(\omega k)}{\mathrm{dn}(\omega,k)}-\frac{\mathrm{sn}(\omega s,k)\mathrm{cn}(\omega s,k)}{\mathrm{dn}(\omega s,k)}\right]\} \\ \eta(s) &= -\frac{2k}{\omega}[\mathrm{cn}(\omega+K,k)-\mathrm{cn}(\omega s+K,k)] = \frac{2kk'}{\omega}\left[\frac{\mathrm{sn}(\omega,k)}{\mathrm{dn}(\omega,k)}-\frac{\mathrm{sn}(\omega s,k)}{\mathrm{dn}(\omega s,k)}\right]\end{aligned} \tag{71}$$

The expanded form of the solution is useful for calculation purposes because it avoids numerical problems for the special case when $\alpha = \pi$ and therefore $k = 1$ and $K(1) = \infty$. For this case, because $\mathrm{sn}(z,1) = Z(z,1) = \tanh z$ and $\mathrm{cn}(z,1) = \mathrm{dn}(z,1) = 1/\cosh z$ (Armitage et al., 2006, p. 16), from (68)–(71), we obtain a trivial solution. When $\alpha = 0$, then $k = 0$ and therefore $\mathrm{sn}(z,0) = \sin z$, $\mathrm{cn}(z,0) = \cos z$, and $\mathrm{dn}(z,0) = 1$, $Z(z,0) = 0$ and $E = K = \pi/2$ (Armitage et al., 2006, p. 15). Substituting these values into Eqs. (68)–(71) also yields a trivial solution.

The present solution given by Eqs. (68)–(71) contains as an argument a complete elliptic integral K, while the solution functions given in Zakharov et al. (2004) contain as an argument the incomplete elliptic integral of the first type. In the present solution, the direction of force γ is also given explicitly by Eq. (70) while in Zakharov et al. (2004) (Eq. (9)), the explicit expression for load parameter ω is given. As we show below, this expression is the solution of Eq. (68) when ω is taken as the unknown.

5. Numerical examples

For the numerical calculations, we wrote a computer program where we use a slightly modified subroutine JELP from Zhang and Jin (1996) to calculate the Jacobian elliptic functions and the ACM Algorithm 577 (Carlson and Notis, 1981) to calculate the Legendre elliptic integrals and Z-function. All numerical computations were executed in a double precision numerical model.

Table 1 shows a comparison of some of the calculations obtained using both our program and the Maple program, where the number of digits was set to 14. The calculations match to 11 digits.

Tables 2–4 present comparisons of the results obtained using the present method and the numerical solution of the problem.

Table 1
Comparison of results of calculated tip coordinates (x_0, y_0), tip tangent angle ϕ_0 and root curvature κ_1 for $\alpha = 90°$, $\kappa_0 = 0$ and various values of load parameter ω .

ω	x_0	y_0	ϕ_0/π	κ_1/ω	Difference with Maple $\times 10^{-12}$			
					Δx_0	Δy_0	$\Delta\phi_0$	$\Delta\kappa_1$
1	0.935645669481	0.320641994675	0.157844984090	0.975510043970	0.33	−0.12	−0.14	0.44
5	0.461585556493	0.102962763465	0.740348529768	−1.206829444100	−0.18	−0.42	−0.12	−0.10
10	0.195867673290	0.457111103310	0.801395679728	1.080955458240	−0.33	−0.05	−0.54	3.40
50	0.457047600338	0.010527023263	0.527000611134	−1.411668886800	−0.22	−0.30	0.24	2.70
100	0.002095409686	0.457488959373	0.997706928372	0.120031951352	−0.03	0.04	−0.32	−1.53

Table 2
Comparison of results of calculated coordinates (x, y), tangent angle ϕ and curvature κ, when $\omega = 10$, $\kappa_0 = 0$ and $\alpha = 90°$, and various values of s.

s	x	y	ϕ/π	κ/ω	Difference with dopri5 $\times 10^{-6}$			
					Δx_0	Δy_0	$\Delta\phi_0$	$\Delta\kappa_0$
0.0	0.1958677	0.4571111	0.8013957	0.0000000	−0.04	−0.47	0.23	0.00
0.2	0.2514655	0.2948450	0.2359386	1.3992359	−0.16	−0.42	−0.54	0.07
0.4	0.0729499	0.3363053	−0.1850488	−0.2917977	−0.12	−0.14	−0.34	0.13
0.6	−0.0809303	0.2925161	0.4923433	−1.2848374	−0.05	−0.07	0.01	−0.37
0.8	0.0431836	0.1453901	0.7472228	0.5820115	−0.06	0.00	0.11	−0.36
1.0	0.0000000	0.0000000	0.0000000	1.0809555	0.00	0.00	0.00	0.72

Table 3
Comparison of results of calculated tip coordinates (x_0, y_0), tip tangent angle ϕ_0 and root curvature κ_1 for $\alpha = 90°$, $\omega = 5$ and various values of free end curvature κ_0.

κ_0	x_0	y_0	ϕ_0/π	κ_1/ω	Difference with *dopri5* $\times 10^{-9}$			
					Δx_0	Δy_0	$\Delta\phi_0$	$\Delta\kappa_1$
5	0.446415423	−0.313062861	0.710386283	−8.029354398	0.18	0.32	1.27	2.60
7.5	0.113376313	0.315858110	1.802376703	5.211869664	−1.81	0.93	0.45	28.96
10	0.015288729	0.084345999	3.183130184	8.531987832	−0.51	0.01	0.41	3.08
15	0.006704371	0.073344605	4.792504287	15.979160875	0.18	0.41	0.07	3.35
−5	−0.272119971	−0.055314289	1.145431732	1.715272828	1.57	−1.71	0.32	3.83
-7.5	−0.352524470	0.192348943	−1.728937144	−9.688433940	2.83	−0.52	1.20	−9.31
−10	0.110036846	−0.322462967	−2.850046317	−8.792437532	−0.04	0.33	0.05	0.96
−15	0.105702957	−0.134393526	−4.673781913	−13.500678911	−0.81	−0.07	0.11	−3.11

Table 4
Comparison of results of calculated tip coordinates (x_0, y_0), tip tangent angle ϕ_0 and root curvature κ_1 for case $k = 1$ and various values of α and ω. For the analytical calculation, Eqs. (63) and (64) were used.

α (deg)	ω	x_0	y_0	ϕ_0/π	κ_1/ω	Difference with *dopri5* $\times 10^{-9}$			
						Δx_0	Δy_0	$\Delta\phi_0$	$\Delta\kappa_1$
90	1	0.498143105	0.708358790	0.575343418	1.986009816	−0.19	−0.16	0.12	0.35
	5	0.334240815	0.248627803	1.479290239	0.325250796	−1.02	1.81	1.68	38.28
−90	1	0.880845859	0.386135102	0.307464029	0.595690757	−0.07	−0.27	0.01	−0.16
	5	0.885926529	0.270736769	0.496446463	0.055818546	2.55	−3.75	−0.81	−13.24

By following the idea of Shvartsman (2007), we executed the integration in two steps. First, the initial value problem of Eqs. (16) and (17) is solved. The results of the integration are a cantilever fixed end point curvature $\kappa_1 = \kappa(1)$ and the force angle $\gamma = \phi(1)$. With these data and by changing the orientation with $s \to 1 - s$, Eqs. (1), (2), (4), (6), and (9) become

$$\frac{dx}{ds} = \cos\phi, \quad \frac{dy}{ds} = \sin\phi, \quad \frac{d\phi}{ds} = \kappa,$$
$$\frac{d\kappa}{ds} = -\omega^2 \sin(\phi + \gamma), \quad s \in [0, 1] \tag{72}$$

and the associated initial conditions are

$$x(0) = y(0) = 0, \quad \phi(0) = 0, \quad \kappa(0) = \kappa_1 \tag{73}$$

This initial value problem can also be solved numerically without iteration. Our second step is different from the step proposed in Shvartsman (2007), where the Simpson integration is used to obtain a beam shape, presumably requiring storing of the data for $\phi(s)$ from the first integration step. For the numerical integration, we use subroutine *dopri5*, which implements an explicit Runge–Kutta method on the order of 4–5 with stepsize control (Hairer et al., 1993). The results of calculating the beam shape show that when the absolute and relative error of calculation was set to 10^{-7}, the results of analytical and numerical integration agreed to 6 digits. The calculations shown in Tables 3 and 4 were obtained by setting the absolute and relative errors of calculation to 10^{-9}. For these cases, the results match to within 8 digits. The shapes of the deformed cantilever shown in Figs. 3 and 4 correspond to the cases presented in Tables 3 and 4, respectively.

In Table 5, we present the results of calculating the tip angle and tip coordinates for $\alpha = 90°$ that were obtained by several authors. The results obtained by Shvartsman (2007) and Rao and Rao (1986) are identical to the results obtained in the present calculation, while the discrepancy with the results given by Mutyalarao et al. (2010) is at most 4%. This discrepancy can be explained by the fact that the authors used the fourth-order Runge–Kutta method with fixed integration step 0.001 for integration.

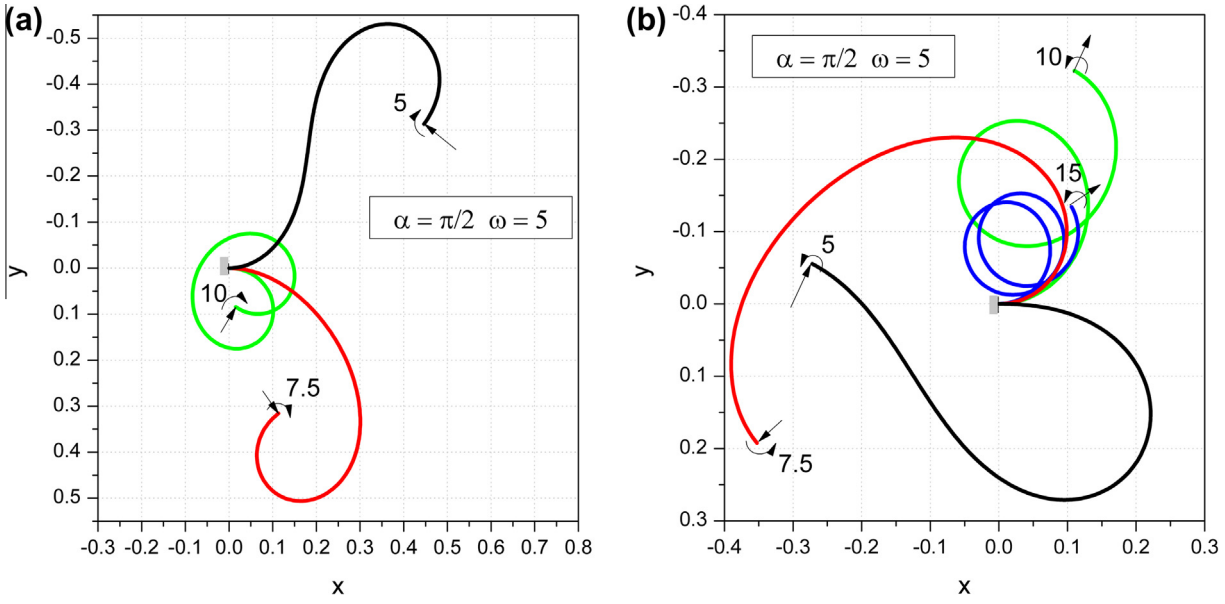

Fig. 3. Cantilever shapes for various values of free end curvature κ_0 when $\alpha = 90°$ and $\omega = 5$.

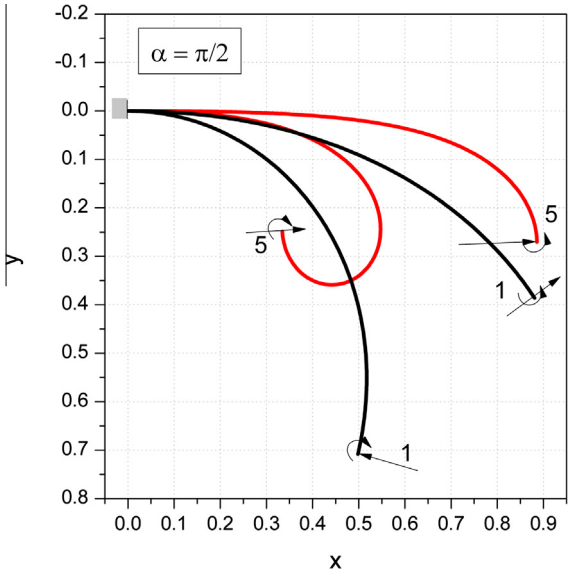

Fig. 4. Cantilever shapes when $\alpha = 90°$, $\kappa_0 = \sqrt{2}\omega$ and various values of ω.

6. Analysis of deformed cantilever base curve

In this section, we give a detailed analysis of a deformed cantilever base line curve where the ultimate goal is to classify its possible forms. Historically, such an analysis was first given by Truesdell and Euler (1960, pp. 199–213) using only integrals and function series expansions. He showed that a deformed cantilever is a part of an infinite periodic curve that can be called elastic. Later, the analysis was performed using Jacobi's elliptic functions, as given by Love (1944, pp. 386–387); using the elliptic integral, by Popov (1986) (chapter 4); and more recently by Antman (1995, pp. 98–100), who provided only a qualitative analysis based on the phase portrait of Eq. (16) in the (φ, κ) plane. These authors considered only a rod subject to a force. More general considerations of possible shapes of elastica were given by Goss (2003) and Sachkov (2008). Some experimental verification of the analytical results is provided in these works and in Sachkov and Levyakov (2010).

The analysis is based on the determination of the cantilever base curve inflection points. By definition, the inflection point is a point where $\kappa(s) = 0$. The curvature has a relative extreme at points where $\frac{d\kappa}{ds} = 0$. Following Zakharov et al. (2004), we call these points compression points (Fig. 5).

6.1. Force dominant case. Inflectional elastic

In what follows, we assume that $k \neq 0$ and the angle corresponding to k is

$$\alpha' = 2\sin^{-1} k \tag{74}$$

Clearly, when $\kappa_0 = 0$, then $\alpha' = \alpha$.

6.1.1. Elastica

To obtain the simplest form of parametric equations of elastic, we introduce a new parameter σ defined by

$$\sigma = \omega s + C \tag{75}$$

and translate the coordinate system into the point $s_0 = -C/\omega$. The parametric equations of elastica are then shown by Eq. (44).

$$\begin{aligned} \overline{\xi} &\equiv \omega[\xi(s_0) - \xi(s_0 + \sigma/\omega)] = \left(\frac{2E}{K} - 1\right)\sigma + 2Z(\sigma, k) \\ \overline{\eta} &\equiv \omega[\eta(s_0) - \eta(s_0 + \sigma/\omega)] = 2k[1 - \mathrm{cn}(\sigma, k)] \end{aligned} \tag{76}$$

Because function cn has a period $4K$ and function Z has a period $2K$, the elastica is a periodic function with period $4K$, and its single wave is given by $0 \leqslant \sigma < 4K$. We see that the shape of the elastica depends only on k and that ω plays a role of scale. In this new parameterization, the tangent angle and the curvature are given by Eqs. (35) and (36)

$$\varphi(\sigma) = 2\sin^{-1}[k\,\mathrm{sn}(\sigma, k)], \quad \overline{\kappa} \equiv \frac{\kappa(\sigma)}{\omega} = -2k\,\mathrm{cn}(\sigma, k) \tag{77}$$

and the inflection σ_n and the compression points σ'_n are at

$$\sigma_n = (2n+1)K, \quad \sigma'_n = 2nK \quad n \in Z \tag{78}$$

According to these calculations, we see that the arc length between successive inflection/compression points is $2K$ and that the arc length of a single wave is $4K$. Each elastic wave contains three com-

Table 5
Comparison of results of calculated tip of tangent angle ϕ_0 and tip coordinates (x_0, y_0) for $\alpha = 90°$ obtained by other authors.

ω^2	ϕ_0(deg)	x_0	y_0	Present			Reference
				ϕ_0 (deg)	x_0	y_0	
0.7010	20[a]	0.9678	0.2292	20.000435	0.967807	0.229225	Rao and Rao (1986)
2.1755	60[a]	0.7312	0.6082	60.001213	0.731196	0.608173	
4.9872	120[a]	0.1742	0.7810	119.999711	0.174160	0.781038	
2[a]	55.48	0.7674	0.5738	55.475997	0.767362	0.573839	Shvartsman (2007)
13.75[a]	180	0.0000	0.4570	180.000000	−0.000014	0.456953	
36[a]	55.64	0.2855	−0.4546	55.629426	0.285341	−0.454598	
220.006	0[a]	−0.000060	−0.457523	0.000000	0.000000	−0.456947	Mutyalarao et al. (2010) Table 2
190.565	30[a]	0.175045	−0.450477	30.000709	0.176352	−0.450321	
79.054	60[a]	0.456241	−0.086106	59.999350	0.451377	−0.089691	

[a] Indicates the input data that the authors used for calculation.

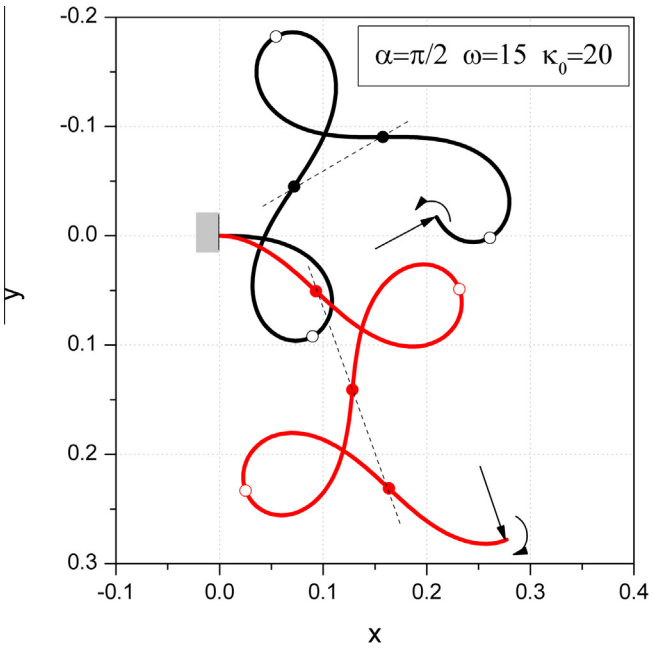

Fig. 5. Inflection (solid circles) and compression points (hollow circles) for two cases with opposite senses of the applied tip moment.

pression points and two inflection points, where the inflection point lies halfway between successive compression points. All of the inflection points lie on the line $\overline{\eta} = 2k$, and the compression points alternate between the lines $\overline{\eta} = 0$ and $\overline{\eta} = 4k$. All lines of the form $\overline{\eta} = c$ are in the space coordinates given by

$$x\sin\gamma + y\cos\gamma = \eta(s_0) - \frac{c}{\omega} = \frac{2k[1 - \mathrm{cn}(\omega + C, k)] - c}{\omega} \tag{79}$$

At inflection points, the value of the tangent angle is

$$\varphi(\sigma_n) = (-1)^{n-1}\alpha' \tag{80}$$

and at compression points, the curvature is maximal.

$$\overline{\kappa}_{\max} = |\overline{\kappa}(\sigma_n')| = 2k \tag{81}$$

6.1.2. Dimensions

The horizontal distance $\Delta\overline{\xi}_c$ and the vertical distance $\Delta\overline{\eta}_c$ (twice the amplitude of the wave) between two successive compression points are given by Eqs. (76) and (78).

$$\Delta\overline{\xi}_c \equiv \overline{\xi}(2K) - \overline{\xi}(0) = 2(2E - K), \quad \Delta\overline{\eta}_c \equiv \overline{\eta}(2K) - \overline{\eta}(0) = 4k \tag{82}$$

When k increases, the elastica begins to form loops. The loop extreme points in the horizontal direction are obtained from the condition $\frac{d\overline{\xi}}{d\sigma} = 1 - 2\mathrm{dn}^2(\sigma, k) = 0$, provided that $k \geqslant \sqrt{2}/2$ or $\alpha' \geqslant \pi/2$. At the interval $0 \leqslant \sigma \leqslant 4K$, this condition leads to four values of parameters ζ, $2K - \zeta$, $2K + \zeta$, and $4K - \zeta$ where

$$\zeta = \mathrm{dn}^{-1}\left(\frac{\sqrt{2}}{2}, k\right) \tag{83}$$

On each wave, we have two possible loops. The loop width $\Delta\overline{\xi}_t$ and the vertical distance between successive extreme points $\Delta\overline{\eta}_t$ are

$$\begin{aligned} \Delta\overline{\xi}_t &\equiv \overline{\xi}(\zeta) - \overline{\xi}(-\zeta) = 2\left(\frac{2E}{K} - 1\right)\zeta + 4Z(\zeta, k) \\ \Delta\overline{\eta}_t &\equiv \overline{\eta}(2K - \zeta) - \overline{\eta}(\zeta) = 4k\,\mathrm{cn}(\zeta, k) \end{aligned} \tag{84}$$

Two examples of calculations using these formulas are shown in Fig. 7 (cases a and b).

6.1.3. Intersection points

For the elastic to have self-intersection points, we must have $\xi(\sigma_1) = \xi(\sigma_2)$, $\eta(\sigma_1) = \eta(\sigma_2)$ and $\sigma_1 \neq \sigma_2$. Following Eq. (76), this requirement leads to a system of two nonlinear algebraic equations for unknowns σ_1 and σ_2.

$$\begin{aligned} 0 &= \left(\frac{2E}{K} - 1\right)(\sigma_2 - \sigma_1) + 2[Z(\sigma_2, k) - Z(\sigma_1, k)], \\ \mathrm{cn}(\sigma_1, k) &= \mathrm{cn}(\sigma_2, k) \end{aligned} \tag{85}$$

By introducing the new variables

$$\sigma_1 = \zeta \quad \text{and} \quad \sigma_2 = -\zeta + 4qK \quad \zeta \in (0, K) \quad (q = 0, \pm 1, \ldots) \tag{86}$$

the second equation reduces to an identity, and the first equation becomes

$$\Phi_q(\zeta, k) \equiv \left(\frac{2E}{K} - 1\right)(\zeta - 2qK) + 2Z(\zeta, k) = 0 \quad (q = 0, \pm 1, \ldots) \tag{87}$$

The graph of this relationship is shown in Fig. 6 (left). From this graph, for the given value of α', we may obtain from zero up to an infinite number of intersection points. However, only three values of α' are of some interest:

- the value of α' when all of the waves overlap each other ($q = \infty$),
- the value of α' when a wave touches an adjacent wave ($q = 1$), and
- the value of α' when a wave detaches ($q = -1$).

The solution for the overlapping case is obtained by setting $\zeta = K$, so Eq. (87) becomes the equation for the unknown k of the form $K(k) = 2E(k)$. The solution of this equation is $k \approx 0.9089086$, given Euler's $\alpha' \approx 130^0\,42'\,35.7''$ (Euler, 1933, pp 154). This solution may also be obtained by the requirement that all of the inflection

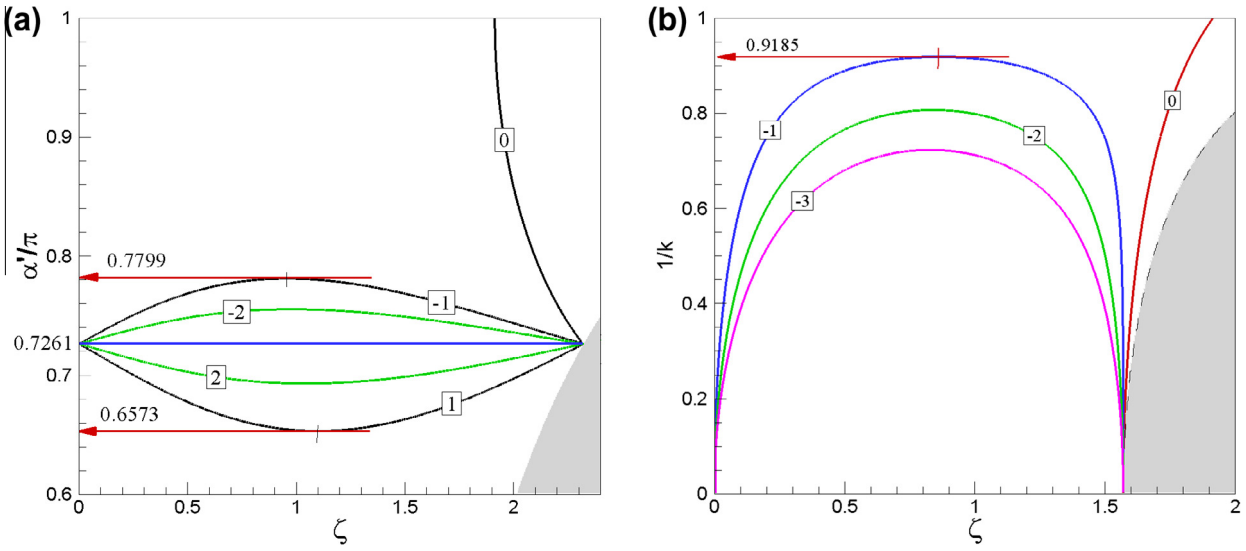

Fig. 6. On the left is the graph of $\Phi_q(\zeta, \sin\frac{\alpha'}{2}) = 0$ given by Eq. (87) for different values of q. On the right is the graph of the relationship given by Eq. (106). In the dark regions, $\zeta > K$.

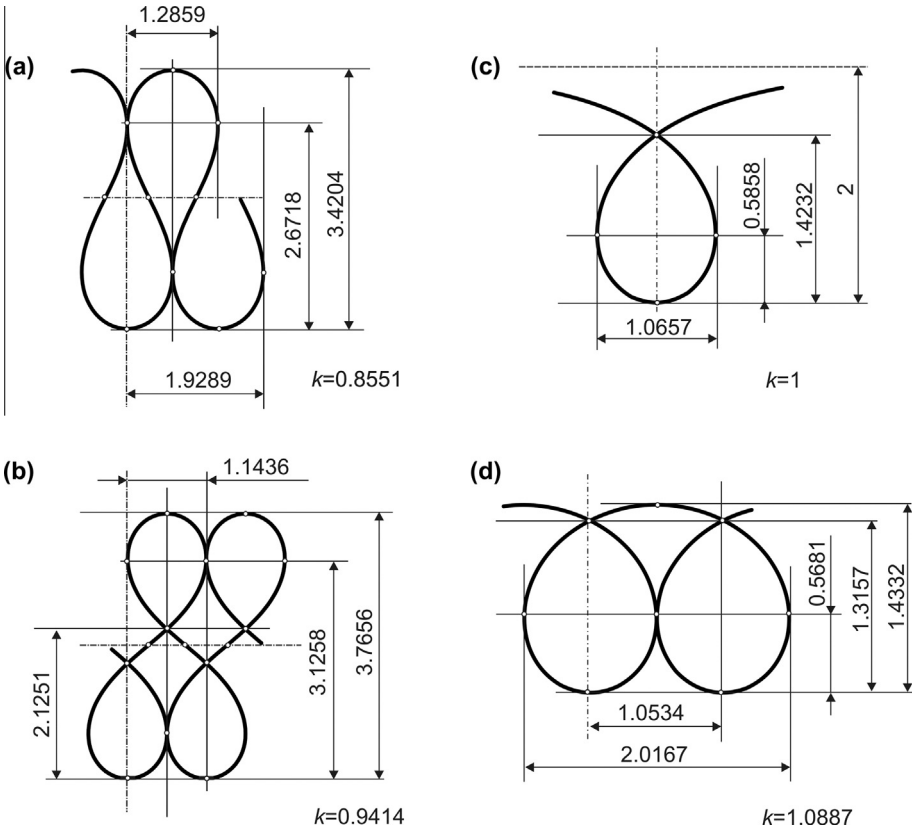

Fig. 7. Some characteristic dimensions of elastica for various values of k. To obtain physical dimensions, the values for cases a, b and c should be multiplied by L/ω, while the values for case d should be multiplied by $L/k\omega$. The values for case a and c agree with those given by Goss (Goss, 2003, Fig. 4.16 and Fig. 4.9).

and compression points coincide; Eq. $(82)_1$ therefore becomes $\Delta\bar{\xi}_c = 0$, which yields the equation $K = 2E$.

The values of α' for attachment and detachment are obtained by solving the system consisting of Eq. (87) and the following equation

$$\frac{\partial \Phi_q}{\partial \zeta} = 1 - 2\mathrm{dn}^2\zeta = 0 \tag{88}$$

The solution of this equation is given by Eq. (83). Substituting Eq. (83) into Eq. (87) yields an equation for unknown k that has the solution $k \approx 0.8550924$ for $q = 1$ and the solution $k \approx 0.9414031$ for $q = -1$. The first k yields the attachment value $\alpha' \approx 117^0 32' 23.6''$ and the corresponding parameter $\zeta \approx 1.0997400$, and the second k yields the detachment value $\alpha' \approx 140^0 34' 37.5''$ and the parameter $\zeta \approx 0.9554893$. The shape

and dimensions of the elastica for these values of α' are shown in Fig. 7 (cases a and b).

The parameter ζ that locates the wave self-intersection point for a given k is the solution of the Eq. (87) when $q = 0$ and is the solution of Eq. (89), below.

$$\left(\frac{2E}{K} - 1\right)\zeta + 2Z(\zeta, k) = 0, \quad \zeta \in (0, K) \tag{89}$$

At the given interval $Z \geqslant 0$, we therefore obtain the solution only when $2E < K$, that is, when $\alpha' > 130.7°$. This solution can also be observed on the graph in Fig. 6. The parameters that define intersection points on a single wave are then given by ζ, $2K - \zeta$, $2K + \zeta$, and $4K - \zeta$. The distances in the coordinate directions between successive intersection points are given by Eq. (84), where ζ is the solution of Eq. (89).

6.1.4. Cantilever

To determine the number of inflection m and compression points m' on a cantilever, we first note that the new parametrization of the end points of the cantilever is determined by

$$\sigma_0 = C, \quad \sigma_1 = C + \omega \tag{90}$$

Based on the definition of C given by Eq. (39), we distinguish three cases.

- *Case when* $\kappa_0 < 0$. In this case, we have $0 < C \leqslant K$, so the number of inflection points m and the number of compression points m' are given by

$$m = 1 + \text{floor}\left(\frac{\omega - K + C}{2K}\right), \quad m' = \text{floor}\left(\frac{1}{2} + \frac{\omega - K + C}{2K}\right) \tag{91}$$

In the limit when $\kappa_0 \to 0$, the cantilever free end becomes an inflection point, and when $C \to 0$, the free end becomes a compression point.

- *Case when* $\kappa_0 > 0$. In this case, $K < C \leqslant 2K$, the number of inflection points m and the number of compression points m' are given by

$$m = \text{floor}\left(\frac{1}{2} + \frac{\omega - 2K + C}{2K}\right), \quad m' = 1 + \text{floor}\left(\frac{\omega - 2K + C}{2K}\right) \tag{92}$$

Again, in the limit when $\kappa_0 \to 0$, we have $C = K$, and the free end becomes an inflection point. When $\alpha = 0$, we have $C = 2K$, so the free end point becomes a compression point.

- *Case when* $\kappa_0 = 0$. The number of inflection points m and the number of compression points m' are given by

$$m = 1 + \text{floor}\left(\frac{\omega}{2K}\right), \quad m' = \text{floor}\left(\frac{1}{2} + \frac{\omega}{2K}\right) \tag{93}$$

where a cantilever free end is the first inflection point. From this relation we see that

- when ω is constant and α increases, then K also increases and m therefore decreases;
- when α is constant and ω increases, then m also increases;
- when m is constant, then ω and α cannot be independent.

6.2. Moment dominant case. Noninflectional elastica

For the moment dominant case, the curvature is given by Eq. (36). Because the function dn has no zeros, a cantilever in this case can have no inflection points (Fig. 8, left)

6.2.1. Elastica

To obtain simple forms of equations of elastica, we translate the coordinate system into the point where $s_0 = -C/(k\omega)$ and introduce the new parameter coordinate σ defined by

$$\sigma = C + k\omega s \tag{94}$$

According to this equation and to Eq. (56), the parametric equations of elastica are

$$\begin{aligned} \overline{\xi} &= k\omega\left[\xi\left(s_0 + \frac{\sigma}{k\omega}\right) - \xi(s_0)\right] = \left[2k^2\left(1 - \frac{E}{K}\right) - 1\right]\sigma - 2k^2 Z(\sigma) \\ \overline{\eta} &= k\omega\left[\eta\left(s_0 + \frac{\sigma}{k\omega}\right) - \eta(s_0)\right] = 2k^2[1 - \text{dn}(\sigma)] \end{aligned} \tag{95}$$

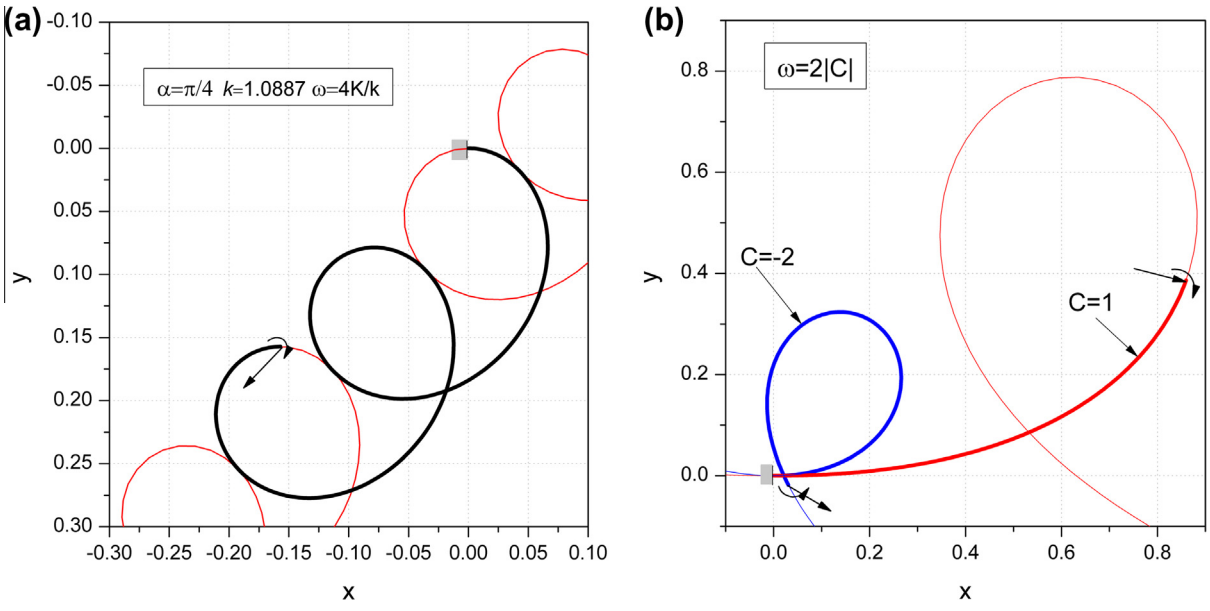

Fig. 8. The examples of noninflectional cantilevers. The thin line represents underlying elastica.

Because both the dn and Z functions have the period $2K$, the elastica also has this period. One wave is thus bounded to $0 \leqslant \sigma \leqslant 2K$, and the scale factor is $k\omega$. The tangent angle and curvature are given by Eqs. (50) and (51).

$$\varphi(s) = -2\mathrm{am}(\sigma, k^{-1}), \quad \overline{\kappa}(s) \equiv \frac{\kappa(s)}{\omega k} = 2\,\mathrm{dn}(\sigma, k^{-1}) \tag{96}$$

Similar expressions with different parameterizations are given by Goss (2003, equations (4.26), (4.28), (4.23) and (4.22)). By definition, at a compression point the curvature has extremes. From condition $\frac{d\kappa}{ds} = 0$, we obtain the equation $\mathrm{sn}(\sigma, k^{-1})\mathrm{cn}(\sigma, k^{-1}) = 0$ using Eq. (51). The parametric coordinates of the compression points are zeros of this equation and are at $\sigma'_n = nK$, where n is any integer. When $\sigma'_n = 2nK$, we have $\frac{d^2\kappa}{ds^2} = -2\omega^3 k < 0$, and therefore the curvature has the maximum

$$\overline{\kappa}_{\max} = 2 \tag{97}$$

When $\sigma'_n = (2n+1)K$, we have $\frac{d^2\kappa}{ds^2} = 2\omega^3\sqrt{k^2-1} > 0$, and therefore the curvature has the minimum

$$\overline{\kappa}_{\min} = 2\sqrt{1-k^{-2}} \tag{98}$$

All of the compression points where the curvature has a maximum lie on the line $\overline{\eta} = 2k\left(k - \sqrt{k^2-1}\right)$, while all of the compression points where curvature is a minimal lie on the line $\overline{\eta} = 0$. All lines of the form $\overline{\eta} = c$ are in space coordinates and are given by

$$x\sin\gamma + y\cos\gamma = \frac{c}{k\omega} - \eta(s_0) = \frac{c - 2k^2[1 - \mathrm{dn}(k\omega + C, k^{-1})]}{k\omega} \tag{99}$$

6.2.2. Dimensions

From Eq. (95), the distance between wave end points is

$$\Delta\overline{\xi}_c = \overline{\xi}(2K) - \overline{\xi}(0) = 2[2k^2(K-E) - K] \tag{100}$$

The two end points coincide when $\Delta\overline{\xi}_c = 0$, and this is possible only when $k = \infty$, i.e., in the case with no applied force or when the elastica becomes a circle. The wave extreme points in the $\overline{\xi}$ direction are obtained from the condition $\frac{d\overline{\xi}}{d\sigma} = 2\mathrm{sn}^2(\sigma) - 1 = 0$. At the interval $\sigma \in (0, 2K)$, we have two solutions

$$\sigma_1 = \mathrm{sn}^{-1}\left(\frac{\sqrt{2}}{2}\right), \quad \sigma_2 = 2K - \sigma_1 \tag{101}$$

The distance between two extremes $\Delta\overline{\xi}_t$ in the horizontal direction is

$$\Delta\overline{\xi}_t = \overline{\xi}(\sigma_2) - \overline{\xi}(\sigma_1) = 2\left[2k^2\left(\frac{E}{K} - 1\right) + 1\right](1 - \sigma_1) + 4k^2 Z(\sigma_1) \tag{102}$$

and the distance $\Delta\overline{\eta}_t$ between the extreme point and the compression point is

$$\Delta\overline{\eta}_t = \overline{\eta}(\sigma_1) = \overline{\eta}(\sigma_2) = k\left(2k - \sqrt{4k^2-2}\right) \tag{103}$$

The wave extremes in the $\overline{\eta}$ direction are obtained by solving $\frac{d\overline{\eta}}{d\sigma} = 2\mathrm{sn}(\sigma)\mathrm{cn}(\sigma) = 0$. At the interval $\sigma \in [0, K)$, we have two possible values

$$\sigma_1 = 0, \quad \sigma_2 = K \tag{104}$$

The height of wave $\Delta\overline{\eta}_c$ is therefore

$$\Delta\overline{\eta}_c = \overline{\eta}(K) - \overline{\eta}(0) = 2k\left(k - \sqrt{k^2-1}\right) \tag{105}$$

6.2.3. Self-intersection points

Similar to the inflectional case, we set intersection points that are at $\sigma_1 = \zeta$ and $\sigma_2 = -\zeta + qK$, where q is an integer. According to Eq. (95), the parameter ζ is the solution of the following equation:

$$\Phi \equiv \left[2k^2\left(\frac{E}{K} - 1\right) + 1\right]\left(\zeta - \frac{qK}{2}\right) + 2k^2 Z(\zeta) = 0 \qquad (0 < \zeta < K) \tag{106}$$

For the case $q = 0$, this equation reduces to

$$\left[2k^2\left(1 - \frac{E}{K}\right) - 1\right]\zeta - 2k^2 Z(\zeta) = 0 \tag{107}$$

At the given interval $Z \geqslant 0$, the first term is also positive, so in any case, we can obtain the intersection point. This point can also be observed on the graph in Fig. 6 (right). To obtain the case when successive waves touch, we solve $\frac{\partial\Phi}{\partial\zeta} = 1 - 2\mathrm{sn}^2(\zeta, k^{-1}) = 0$, which gives $\zeta = \mathrm{sn}^{-1}\left(\frac{\sqrt{2}}{2}, k^{-1}\right)$. For $q = -1$, Eq. (106) gives the value $k \approx 1.08874$. In this case, the intersection point is given by the parameter $\zeta \approx 1.82566$. The shapes and dimensions of elastica for this case are shown in Fig. 7 (case d).

6.2.4. Cantilever

The end points of a cantilever in the new parametrization are given by

$$\sigma_0 = C, \quad \sigma_1 = C + k\omega \tag{108}$$

The number of compression points is therefore

$$m' = \mathrm{floor}\left(\frac{k\omega + C}{K}\right) + \begin{cases} 0 & \alpha < 0 \\ 1 & \alpha > 0 \end{cases} \tag{109}$$

When $\alpha > 0$ (the tip moment has the same sense as the moment produced by the applied force), then the origin is always part of the cantilever. The cantilever in this case contains at least one compression point.

6.3. Case k=1. Homoclinic elastica

6.3.1. Elastica

We introduce the new parameter coordinate σ, which is defined by

$$\sigma = C + \omega s \tag{110}$$

and translate the coordinate system into the point $s_0 = -C/(k\omega)$. From Eq. (64), the parametric equations of the elastica are

$$\begin{aligned} \overline{\xi} &\equiv \omega\left[\xi\left(s_0 + \frac{\sigma}{\omega}\right) - \xi(s_0)\right] = \sigma - 2\tanh(\sigma) \\ \overline{\eta} &\equiv \omega\left[\eta\left(s_0 + \frac{\sigma}{\omega}\right) - \eta(s_0)\right] = 2\left[1 - \frac{1}{\cosh(\sigma)}\right] \end{aligned} \tag{111}$$

Both functions are nonperiodic, so $\sigma \in (-\infty, \infty)$. Apart from parametrization, these formulas are similar to those given by Goss (2003, equations (4.57), (4.58)). The example of homoclinic elastic is shown in Fig. 8 (right).

The tangent angle and the curvature are in the new parametrization given by Eq. (63).

$$\varphi(s) = -2\sin^{-1}[\tanh(\sigma)], \quad \overline{\kappa} \equiv \frac{\kappa(s)}{\omega} = \frac{2}{\cosh(\sigma)} \tag{112}$$

By definition, at the compression points, the curvature has an extreme. The condition gives the equation $\sinh(\sigma) = 0$ $\frac{d\kappa}{ds} = 0$ using $(63)_2$. This equation has only one zero at $\sigma' = 0$. At this point, we have $\frac{d^2\kappa}{ds^2} = -2\omega^3 < 0$, and therefore the curvature has the maximum

$$\kappa_{\max} = 2 \tag{113}$$

6.3.2. Dimensions

From Eq. (111), we can derive various dimensions of elastica. The wave extreme points in the $\overline{\xi}$ direction are obtained from the condition that $\frac{d\overline{\xi}}{d\sigma} = 1 - 2/\cosh^2\sigma = 0$, thus yielding two values:

$$\sigma_1 = \cosh^{-1}\left(\sqrt{2}\right) \approx 0.88137, \quad \sigma_2 = -\sigma_1. \tag{114}$$

The arc length between extremes is thus

$$\Delta\sigma = \sigma_2 - \sigma_1 = 2\cosh^{-1}\left(\sqrt{2}\right) \approx 1.76275 \tag{115}$$

The horizontal distance between extremes is

$$\Delta\overline{\xi}_t = \overline{\xi}(\sigma_1) - \overline{\xi}(\sigma_2) = 2\left(\sqrt{2} - \cosh^{-1}\sqrt{2}\right) \approx 1.06568 \tag{116}$$

The distance between the compression point and the extreme is

$$\Delta\overline{\eta}_t = \overline{\eta}(\sigma_1) - \overline{\eta}(0) = 2 - \sqrt{2} \approx 0.58579 \tag{117}$$

In the limit, we have

$$\lim_{\sigma\to\pm\infty}[\overline{\eta}(\sigma) - \overline{\eta}(0)] = 2 \tag{118}$$

The shape and dimensions of homoclinic elastica are shown in Fig. 7 (case c).

6.3.3. Self-intersection point

We set intersection points at $\sigma_1 = \zeta$ and $\sigma_2 = -\zeta$. According to Eq. (111), we then obtain the following equation

$$\zeta - 2\tanh\zeta = 0 \tag{119}$$

which has the solution $\zeta \approx 1.91501$ and gives $\overline{\eta} \approx 1.42316$.

6.3.4. Cantilever

The end points of a cantilever are given by

$$\sigma_0 = C \quad \text{and} \quad \sigma_1 = C + \omega \tag{120}$$

so the cantilever contains the compression point only if $C \leqslant 0$, i.e., when $\alpha > 0$. In the special case when $C = -\zeta$ and ζ is the solution of Eq. (119), according to Eq. (65) we obtain $\alpha \approx 0.81374\pi$ or $\alpha = 146^0 28' 23.7''$. At this angle, according to Eq. (120), a cantilever deforms into a closed loop when $\omega = 2\zeta$.

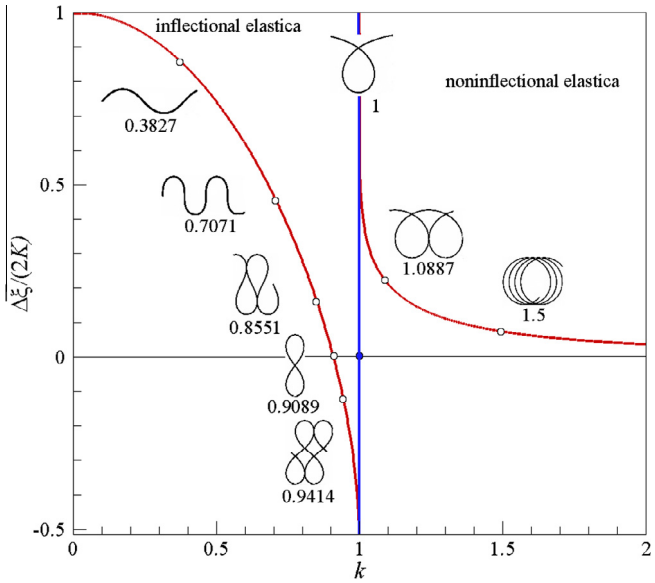

Fig. 9. Various forms of elastica as a function of k and the distance between compression points.

The results of this section are summarized on the graph in Fig. 9, where various forms of elastica as a function of k and the distance between compression points are shown.

7. Various force load conditions

In this section, we discuss various problems that can be set using Eq. (20), where we discuss only the cases of applied force, i.e., cases with $\kappa_0 = 0$. In particular, we have the following problems:

1. When ω and α are given, then Eq. (20) is the explicit expression for γ, so we have only one solution. This problem is known as the follower load problem. In this case, the force is nonconservative because its line of action depends on a deformed cantilever shape.
2. When α and γ are given, then Eq. (20) represents the equation for an unknown ω. Because the equation is (in general) nonlinear, we may expect multiple solutions, i.e., multiple equilibrium configurations. As shown below, we in fact obtain infinitely many solutions (Rao and Rao, 1986). We call this problem a load parameter problem.
3. When ω and γ are given, then Eq. (20) represents the equation for unknown α. This is a conservative load problem and has a finite number of solutions (Navaee, 1992), Batista and Kosel, 2005.

7.1. Follower load

When ω and α are given, we have the follower load problem. In this case, Eq. (70) (when $|\alpha| < \pi$) gives an explicit and unique solution for γ. Two examples are shown in Figs. 10 and 11. In the first of these figures, the load parameter ω increases and α is constant. In the second figure, the situation is the opposite. All other possibilities of input data yield multiple solutions of the nonlinear Eq. (70) that is a finite or infinite number of equilibrium configurations. However, each of the configurations can be reached by some equivalent follower load.

We now consider some particular solutions of Eq. (70) that follow the form of special values of the Jacobian elliptic functions.

1. When $\omega_n = (2n - 1)K$ $(n = 1, 2, \ldots)$, then the cantilever fixed point is a compression point. From Eq. (70), we have
$$\gamma = 0 \tag{121}$$
which means that the force acts in the horizontal direction. The free point tangent angle and free point coordinates are
$$\phi_0 = \alpha, \quad x_0 = 2E/K - 1, \quad y_0 = (-1)^n \frac{2k}{(2n+1)K} \tag{122}$$
We see that x_0 is independent of a particular load and that y_0 tends to zero with an increasing load.
2. When $\omega_n = 2(2n - 1)K$ $(n = 1, 2, \ldots)$, the cantilever shape is formed by n - 1 waves, followed by a half wave. Equation (70) in this case gives
$$\gamma = -\alpha \tag{123}$$
The cantilever free point tangent angle and coordinates in this case are
$$\phi_0 = 2\alpha \qquad x_0 = (2E/K - 1)\cos\alpha \qquad y_0 = (2E/K - 1)\sin\alpha \tag{124}$$
Both cantilever free point coordinates are independent of the particular value of the load parameter.

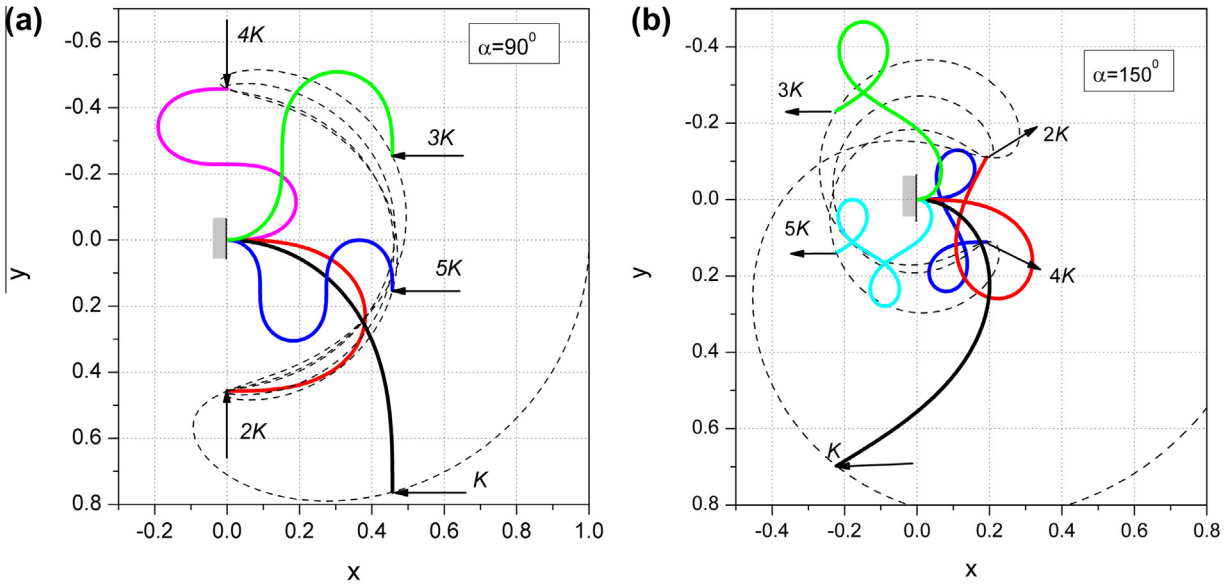

Fig. 10. Path of beam tip point (dotted line) and some correspondent beam shapes when α is given and ω increases. With an increasing ω, the number of waves of a cantilever also increases.

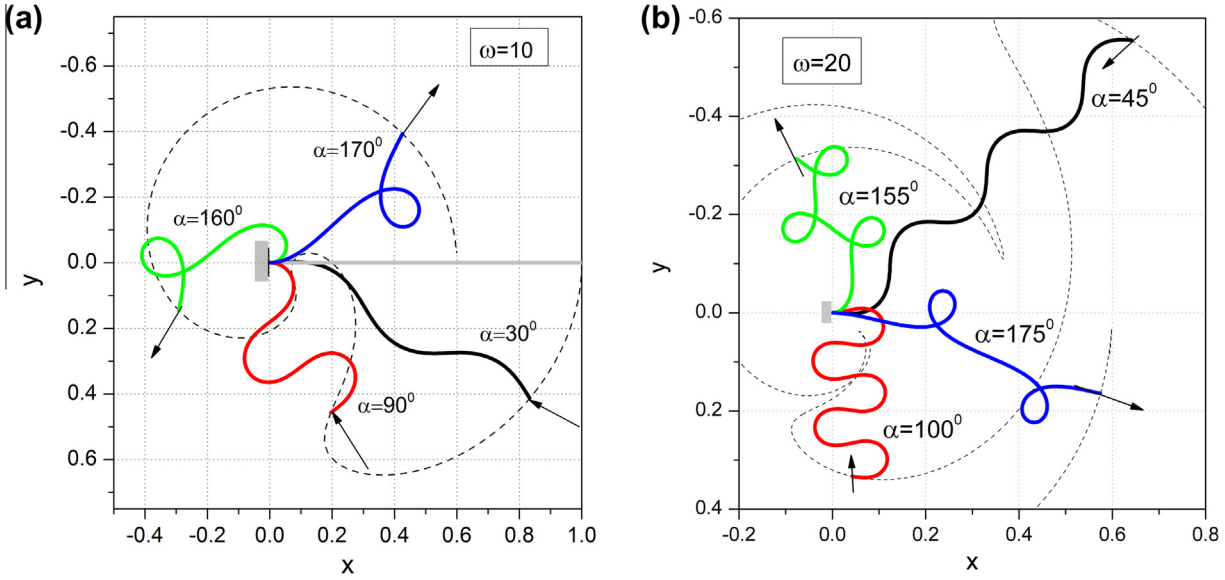

Fig. 11. The path of the beam tip point (dotted line) and some correspondent beam shapes when ω is given and α increases. With an increasing α, the number of waves of a cantilever decreases.

3. When $\omega_n = 4nK$ ($n = 1, 2, \ldots$), the cantilever shape is formed by n waves. From Eq. (70), we obtain

$$\gamma = \alpha \tag{125}$$

As in the previous case, the coordinates of tip points are independent of load factor and are given by

$$\phi_0 = 0, \quad x_0 = (2E/K - 1)\cos\alpha, \quad y_0 = -(2E/K - 1)\sin\alpha \tag{126}$$

The described behaviors given by these special solutions may be observed in Fig. 10.

7.2. Load parameter problem

In the case, when α and $|\gamma| \leqslant \alpha$ are given, Eq. (70) becomes the equation for an unknown ω. We rewrite this equation into the following form:

$$\mathrm{sn}(\omega + K) = A, \quad A \equiv \frac{\sin(\gamma/2)}{\sin(\alpha/2)} \tag{127}$$

We note that this problem also covers the problem when the free point tangent angles ϕ_0 and α are given because γ is then given by Eq. (5).

The solution of this equation that is closest to the origin is

$$\omega_0 = K - \mathrm{sn}^{-1}(A, k) \tag{128}$$

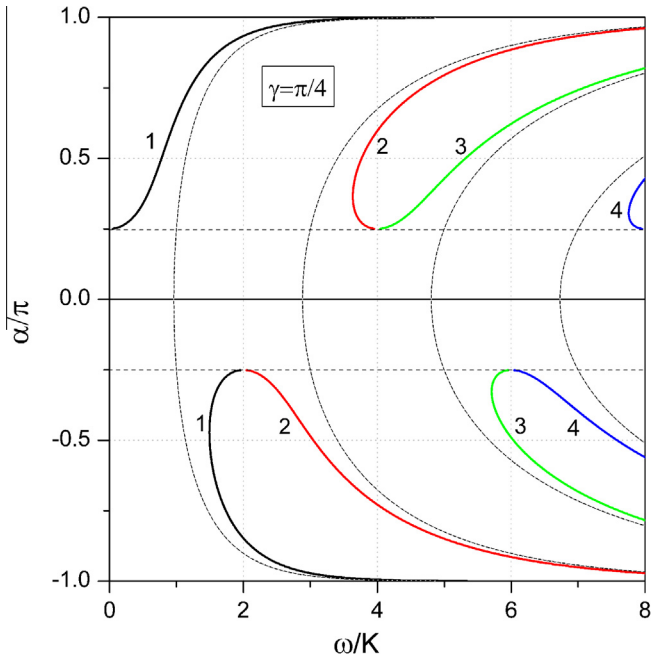

Fig. 12. Graph of (129) for $\gamma = \pi/4$. The dotted curve represents the graph for case $\gamma = 0$.

where $0 \leqslant \omega_0 \leqslant K$. From the periodicity of the function sn, then the infinite sequence of possible solutions follows. We distinguish two cases:

1. When $\gamma \geqslant 0$, we have the sequence of load parameters

$$\begin{aligned} \omega_{2n-1} &= \omega_0 + 4(n-1)K \\ \omega_{2n} &= -\omega_0 + 4nK \qquad (n = 1, 2, \ldots) \end{aligned} \tag{129}$$

2. When $\gamma < 0$, the load parameters are

$$\begin{aligned} &\omega_{2n-1} = -\omega_0 + 2(2n-1)K, \\ &\omega_{2n} = \omega_0 + 2(2n+1)K \quad (n = 1, 2, \ldots). \end{aligned} \tag{130}$$

The load parameters given by Eqs. (129) and (130) can be represented as branches on a bifurcation diagram in a (ω, α) plane, as shown on the graph in Fig. 12. There are two possible uses of the solutions to Eqs. (129) or (130). If we take the constant n (which is also called the wave number because it determines the number of waves that form the cantilever shape), then the solution of the problem is a load parameter that is a continuous function of α. When α is constant, then for each n, we obtain an equilibrium configuration. Examples are shown in Figs. 13 and 14.

7.3. Conservative load

Consider now the case when γ and ω are given and α is unknown, which is also known as the conservative load problem. When γ and ϕ_0 are given, then $\alpha = \gamma + \phi_0$, and the problem is equivalent to the load parameter problem discussed in the previous section.

We rewrite Eq. (70) into the following form

$$\sin\frac{\gamma}{2} = k\,\mathrm{sn}(\omega + K, k), \quad \alpha = 2\sin^{-1}(k) \tag{132}$$

and consider two cases of possible solutions for unknown k, where we assume that $k \neq 0$.

The case when $\gamma = 0$. In this case, the solutions of Eq. (132) are $\omega = (2n-1)K$ and $(n = 1, 2, \ldots)$. For a given ω, we therefore have the equation

$$K(k) = \frac{\omega}{(2n-1)} \quad (n = 1, 2, \ldots) \tag{133}$$

Because $K(k)$ is a monotone function, there is a unique value of k for each n. However, because $K(k) \geqslant \pi/2$ and the right-hand side of Eq. (133) tends to zero with an increasing n, the number of solutions is finite. To determine the number of solutions, we first consider the special case when $\alpha = 0$. In this case $K(0) = \pi/2$, and therefore $\omega_n = (2n-1)\frac{\pi}{2}$ and $(n = 1, 2, \ldots)$. These values of ω represent bifurcation points on (ω, α) plane (Fig. 12). The number of possible equilibrium configurations doubles at each bifurcation point. Thus, if $\omega_n \leqslant \omega < \omega_{n+1}$, then the number of possible equilibrium configurations including the trivial solution is $2n + 1$, where n is

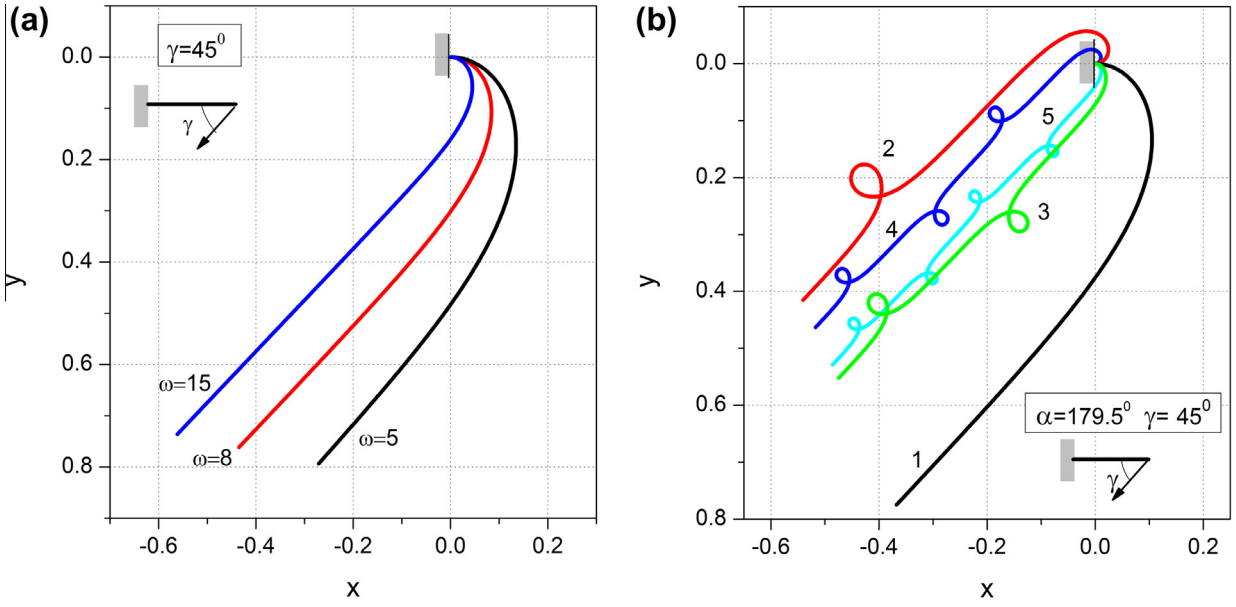

Fig. 13. Cantilever beam equilibrium configurations when $\gamma = 45°$ is calculated using Eq. (129). In the left figure, α is calculated for various load parameters ω when $n = 1$. In the right figure, successive load parameters ω are calculated for a given $\alpha = 179.5°$ and various n. In both cases, a cantilever with increasing ω becomes increasingly straight.

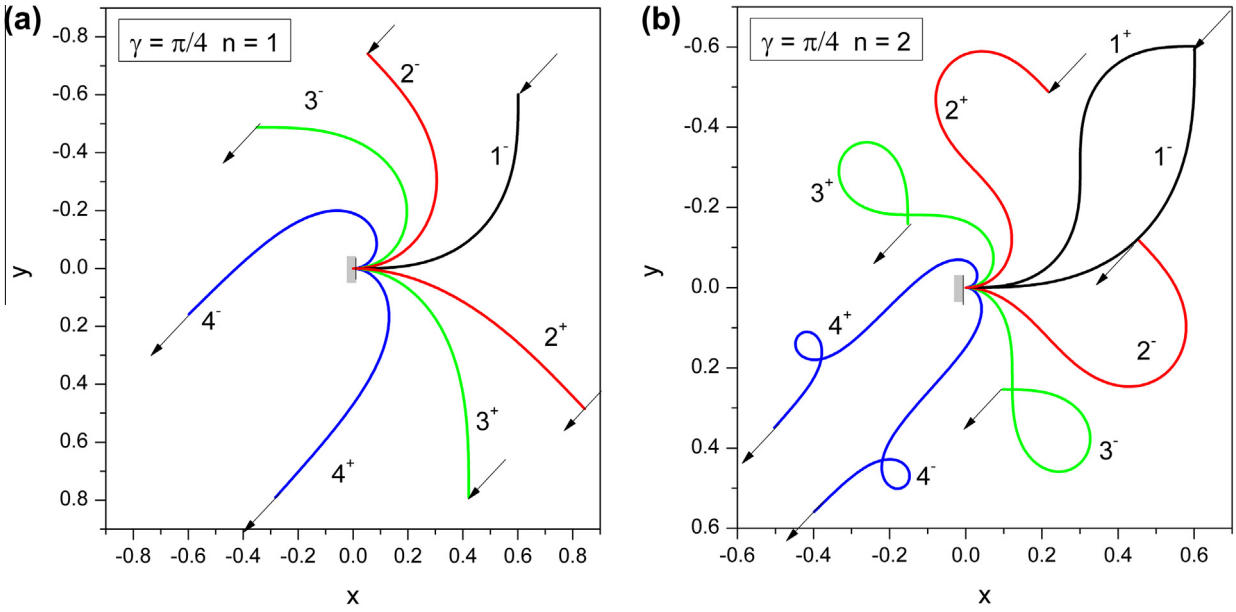

Fig. 14. Equilibrium shapes when $\gamma = \pi/4$, $\alpha/\pi = (\pm 0.25, \pm 0.5, \pm 0.75, \pm 0.99)$ and different n. Load parameters are calculated using Eq. (129). Successive numbers correspond to successive values of α.

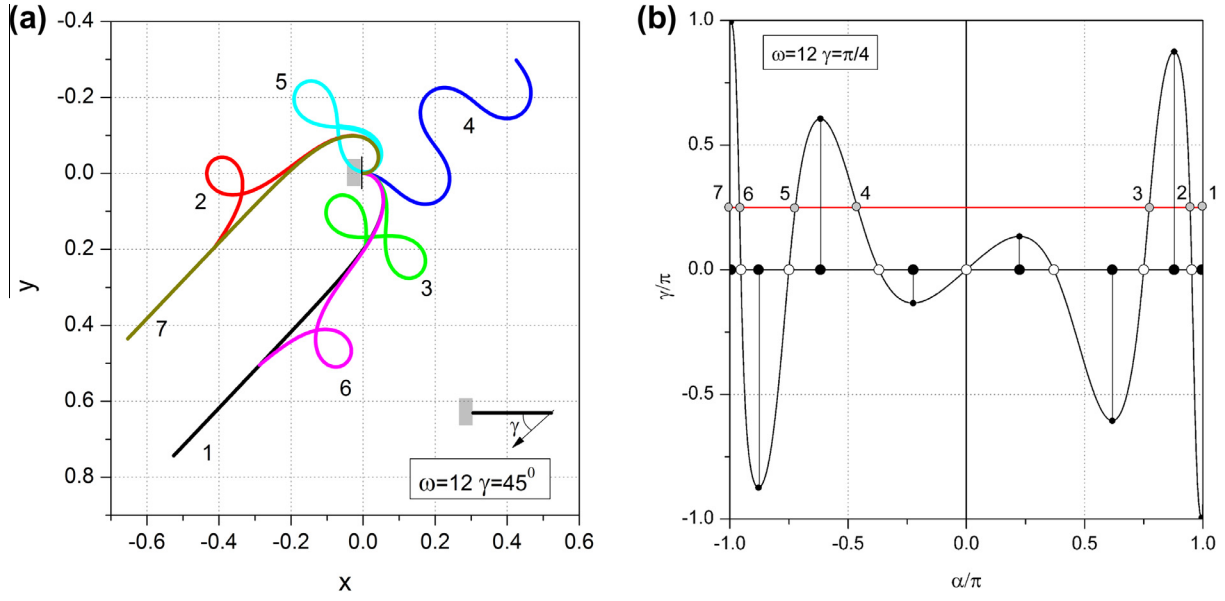

Fig. 15. The cantilever equilibrium shapes when $\omega = 12$ (left). Partition of the interval when $\omega = 12$ (right). For this case, there are 18 intervals. However, the two intervals near each end are very narrow and cannot be displayed well. The number of possible equilibrium configurations is seven.

Table 6
Calculated values of equilibrium configurations for the case of conservative load when $\gamma = 45°$ and $\omega = 12$. The numbers correspond to shapes in Fig. 15.

	α/π	x_0	y_0	ϕ_0/π	κ_1/ω	γ/π
1	0.999989546	−0.525475296	0.743235391	0.749989649	1.847759190	0.249999897
2	0.946286875	−0.412482787	0.195630101	0.696286875	−1.840056050	0.250000000
3	0.773219245	0.006563252	0.195087408	0.523219245	1.711062590	0.250000000
4	−0.460401429	0.425240149	−0.297980044	−0.710401429	1.079837790	0.250000000
5	−0.722781359	−0.068424812	−0.125313200	−0.972781359	−1.643921540	0.250000000
6	−0.959076697	−0.287482201	0.504715675	−1.209076700	1.843287150	0.250000003
7	−0.999976584	−0.653036197	0.435275758	−1.249976600	−1.847759040	0.250000016

$$n = \text{floor}\left(\frac{\omega}{\pi} + \frac{1}{2}\right) \tag{134}$$

For example, for $\omega = 15$, we have $n = 5$ and therefore 11 possible equilibrium configurations.

Eq. (133) does not have an analytical solution and must be solved numerically. The initial estimation of the solution is obtained on the basis of inequality. $\ln 4 \leqslant K + \ln k' \leqslant \pi/2$ (California Institute of Technology, 1953, pp 318), from which it follows that the mth zero falls into the interval

$$\sqrt{1 - e^{\pi} e^{-2\omega/(2m-1)}} \leqslant k_m \leqslant \sqrt{1 - 16 e^{-2\omega/(2m-1)}} \quad (m = 1, 2, \ldots, n) \tag{135}$$

Once we obtain k_m, we have $\alpha_m = 2\sin^{-1}(k_m)$. Zeros for $\alpha < 0$ are then obtained by symmetry.

Case $0 < \gamma < \pi$. When $0 < \gamma < \pi$, then Eq. (132) must be solved numerically, and its roots are to be located in the interval

$$-\pi < \alpha < \pi$$

From the shape of Eq. (70), as shown in Fig. 15 (right), we see that the possible roots lie within intervals that are bounded by roots of Eq. (133), and we have two possible roots within these intervals. These observations suggest that we may use the following procedure to calculate the roots of Eq. (132):

1. Calculate the number of zeros using Eq. (134).
2. Calculate the zeros using estimation (135).
3. Calculate the location of the extreme points between two neighboring zeros and add the extreme values that are on the end of the interval $-\pi < \alpha < \pi$ to them.
4. Partition the interval $-\pi < \alpha < \pi$ to subintervals, where each subinterval is bounded by extreme and zero points.
5. For each such interval, calculate the possible zero of Eq. (132).

An example of a calculation obatined using this procedure is shown in Fig. 15, and some numerical values are given in Table 6.

8. Conclusion

Although the problem discussed in this paper is old and most of the given results are well known, we present some novelties:

1. A new analytical solution of the problem is given in terms of Jacobi elliptical functions and the Jacobi zeta function, where the cantilever load also includes the tip moment;
2. A new analytical expression for calculating various dimensions of elastica is given; and
3. We provide a new efficient procedure for determining all possible equilibrium shapes in the case of the conservative load problem.

In the present paper, the follower load problem, the load parameter problem, and the conservative load problem are treated from a single point of view, namely, as solutions of Eq. (70). The Maple worksheet that implements the solution of these problems is freely available in Batista (2013)

References

Alliney, S., Tralli, A., 1984. Extended variational formulations and Fe models for nonlinear beams under nonconservative loading. Comput. Methods Appl. Mech. Eng. 46 (2), 177–194.

Antman, S.S., 1995. Nonlinear Problems of Elasticity, vol. 17. Springer-Verlag, New York, London, p. 750.

Argyris, J.H., Symeonidis, S., 1981. Non-linear finite-element analysis of elastic-systems under non-conservative loading natural formulation. 1. Quasistatic problems. Comput. Methods Appl. Mech. Eng. 26 (1), 75–123.

Armitage, J.V., Eberlein, W.F., 2006. Elliptic Functions, vol. 13. Cambridge University Press, Cambridge, p. 387.

Audoly, B., Pomeau, Y., 2010. Elasticity and Geometry. Oxford University Press Inc., New York.

Banerjee, A., Bliattacharya, B., Mallik, A.K., 2008. Large deflection of cantilever beams with geometric non-linearity: analytical and numerical approaches. Int. J. Non Linear Mech. 43 (5), 366–376.

Barten, H.J., 1944. On the deflection of a centilever beam. Q. Appl. Math. 2, 168–171.

Batista, M. 2013. Equilibrium Configurations of Cantilever Beam under Terminal Load. Available from: <http://www.maplesoft.com/applications/>.

Batista, M., Kosel, F., 2005. Cantilever beam equilibrium configurations. Int. J. Solids Struct. 42 (16–17), 4663–4672.

Beth, R.A., Wells, C.P., 1951. Finite deeflections of a cantilever-strut. J. Appl. Phys. 22 (6), 742–746.

Bisshopp, K.E., Drucker, D.C., 1945. Large deflection of cantilever beams. Q. Appl. Math. 3 (3), 272–1945.

Bolotin, V.V., 1963. Nonconservative Problems of the Theory of Elastic Stability. Corr. and authorized ed ed., vol. 12, Macmillan, Oxford, p. 324.

Born, M., 1906. *Untersuchungen über die Stabilität der elastischen Linie in Ebene und Raum: unter verschiedenen Grenzbedingungen* (Ph.D. thesis). University of Gottingen.

Bateman Manuscript Project. California Institute of Technology, et al., 1953. Higher Transcendental Functions, vol 2, McGraw-Hill, New York, London.

Carlson, B.C., Notis, E.M., 1981. Algorithm 577 – algorithms for incomplete elliptic integrals [S21]. ACM Trans. Math. Software 7 (3), 398–403.

Clebsch, A., 1862. Theorie der elasticität faster körper. B.G. Teubner, Leipzig.

Coleman, B.D., Swigon, D., 2000. Theory of supercoiled elastic rings with self-contact and its application to DNA plasmids. J. Elast. 60 (3), 173–221.

DeBona, F., Zelenika, S., 1997. A generalized elastica-type approach to the analysis of large displacements of spring-strips. Proc. Inst. Mech. Eng. C J. Mech. Eng. Sci. 211 (7), 509–517.

Euler, L., 1933. Elastic curves. Isis 20 (1), 72–160.

Frisch-Fay, R., 1961. A new approach to the analysis of the deflection of thin cantilevers. Trans. ASME J. Appl. Mech. 28, 87–90.

Frisch-Fay, R., 1962. Flexible bars. Butterworths Scientific Publications, vol. 8. Butterworths, London, p. 220.

Goss, V.G.A., 2003. Snap buckling, writhing and loop formation in twisted rods. In: Center for Nonlinear Dynamics. University Collage London.

Goss, V.G.A., 2009. The history of the planar elastica: insights into mechanics and scientific method. Sci. Educ. 18 (8), 1057–1082.

Greenhill, G., 1892. The Applications of Elliptic Functions, vol. 11. Macmillan, London, p. 357.

Hairer, E., Nörsett, S.P., Wanner, G., 1993. Solving ordinary differential equations. I: nonstiff problems, . Springer Series in Computational Mathematics, second rev. ed., vol. 15. Springer-Verlag, Berlin; London, p. 528.

Hess, W., 1885. Uber die Biegung und Drillung eines unendlich dünnen elastichen Stabes mit zwei gleichen Widerstanden, auf dessen freies Ende eine Kraft und ein um die Hauptaxe ungleichen Widerstandes drehendes Kräftepaar einwirkt. Math. Ann. 25, 1–38.

Hirsch, M.W., Smale, S., Devaney, R.L., 2004. Differential equations, dynamical systems, and an introduction to chaos, . second ed. Pure and Applied Mathematics a Series of Monographs and Textbooks second ed., vol. 14 Academic Press, p. 417.

Howell, L.L., Midha, A., 1994. A method for the design of compliant mechanisms with small-length flexural pivots. J. Mech. Des. 116 (1), 280–290.

Hummel, F.H., Morton, W.B., 1924. On the large bending of thin flexible strips and the measurment of their elasticity. pp. 348–357.

Karlson, K.N., Leamy, M.J., 2013. Three-dimensional equilibria of nonlinear pre-curved beams using an intrinsic formulation and shooting. Int. J. Solids Struct. 50 (22–23), 3491–3504.

Kimiaeifar, A. et al., 2011. Analytical solution for large deflections of a cantilever beam under nonconservative load based on homotopy analysis method. Numer. Methods Partial Differ. Equ. 27 (3), 541–553.

Kuznetsov, V.V., Levyakov, S.V., 2002. Complete solution of the stability problem for elastica of Euler's column. Int. J. Non Linear Mech. 37 (6), 1003–1009.

Lau, J.H., 1982. Large deflections of beams with combined loads. J. Eng. Mech. Div. ASCE 108 (1), 180–185.

Levien, R., 2008. The Elastica: A Mathematical History. University of California at Berkeley.

Levyakov, S.V., Kuznetsov, V.V., 2010. Stability analysis of planar equilibrium configurations of elastic rods subjected to end loads. Acta Mech. 211 (1–2), 73–87.

Linner, A., 1998. Explicit elastic curves. Ann. Global Anal. Geom. 16 (5), 445–475.

Love, A.E.H., 1893, . A Treatise on the Mathematical Theory of Elasticity, first ed., vol. 2. Cambridge university press, London.

Love, A.E.H., 1944, . A Treatise on the Mathematical Theory of Elasticity, fourth. ed., vol. 18. Dover Publications, New York, p. 643.

Maddocks, J.H., 1984. Stability of nonlinearly elastic rods. Arch. Ration. Mech. Anal. 85 (4), 311–354.

Malkin, I., 1926. Formaenderung eines axial gedrueckten duennen stabes. Z. Angew. Math. Mech. 6 (73), 73–76.

Massoud, M.F., 1966. On the problem of large deflexion of cantilever beam. Int. J. Mech. Sci. 8, 141–143.

Mattiasson, K., 1981. Numerical results from large deflection beam and frame problems analyzed by means of elliptic integrals. Int. J. Numer. Methods Eng. 17 (1), 145–153.

Mitchell, T.P., 1959. The nonlinear bending of thin rods. Trans. ASME J. Appl. Mech., 40–43.
Mutyalarao, M., Bharathi, D., Rao, B.N., 2010. Large deflections of a cantilever beam under an inclined end load. Appl. Math. Comput. 217 (7), 3607–3613.
Nallathambi, A.K., Rao, C.L., Srinivasan, S.M., 2010. Large deflection of constant curvature cantilever beam under follower load. Int. J. Mech. Sci. 52 (3), 440–445.
Navaee, S., 1992. Equilibrium-configurations of cantilever beams subjected to inclined end loads. J. Appl. Mech. Trans. ASME 59 (2), 572–579.
Navaee, S., Elling, R.E., 1993. Possible ranges of end slope for cantilever beams. J. Eng. Mech. ASCE 119 (3), 630–637.
Olver, F.W.J., National Institute of Standards and Technology (U.S.), 2010. NIST Handbook of Mathematical Functions. vol. 15, Cambridge University Press, Cambridge, p. 951.
Pflüger, A., 1950. Stabilitätsprobleme der Elastostatik. Springer-Verlag, Berlin, Göttingen, Heidelberg.
Popov, E.P., 1948. Nonlinear Static Problems of Thin Rods. OGIZ, Moscow, Leningrad.
Popov, E.P., 1986. Theory and Calculation of Flexible Elastic Bars. Nauka, Moscow.
Rao, B.N., Rao, G.V., 1986. On the large deflection of cantilever beams with end rotational load. Z. Angew. Math. Mech. 66 (10), 507–509.
Saalschütz, L., 1880. Der belastete stab unter Einwirkung einer seitlichen kraft. B.G. Teubner, Leipzig.
Sachkov, Y.L., 2008. Maxwell strata in the Euler elastic problem. J. Dyn. Control Syst. 14 (2), 169–234.
Sachkov, Y.L., Levyakov, S.V., 2010. Stability of inflectional elasticae centered at vertices or inflection points. Proc. Steklov Inst. Math. 271 (1), 177–192.
Saje, M., Srpcic, S., 1985. Large deformations of inplane beam. Int. J. Solids Struct. 21 (12), 1181–1195.
Saxena, A., Kramer, S.N., 1998. A simple and accurate method for determining large deflections in compliant mechanisms subjected to end forces and moments. J. Mech. Des. 120 (3), 392–400.
Schmidt, R., DaDeppo, D.A., 1971. A survey of literature on large deflections of nonshallow arches. Bibliograpy of finite deflections of straight and curved beams, rings, and shallow arches. J. Ind. Math. Soc. 21 (2), 91–144.
Scott, E.J., Carver, D.R., Manhattan, 1955. On the nonlinear differential equation for beam deflection. Trans. ASME J. Appl. Mech. 22 (77), 245–248.
Shvartsman, B.S., 2007. Large deflections of a cantilever beam subjected to a follower force. J. Sound Vib. 304 (3–5), 969–973.
Tari, H., 2013. On the parametric large deflection study of Euler-Bernoulli cantilever beams subjected to combined tip point loading. Int. J. Non Linear Mech. 49, 90–99.
Timoshenko, S., 1953. History of Strength of Materials: with a Brief Account of the History of Theory of Elasticity and Theory of Structures. McGraw-Hill, New York, p. 452.
Timoshenko, S., Gere, J.M., 1961. Theory of elastic stability. In: Engineering Societies Monographs, second ed. McGraw-Hill Book Company, New York, London, p. 541.
Todhunter, I., Pearson, K., 1960. A History of the Theory of Elasticity and of the Strength of Materials: from Galilei to Lord Kelvin, vol. 2. Dover Publications, New York, p. 3.
Truesdell, C., Euler, L., 1960. The rational mechanics of flexible or elastic bodies, 1638–1788: introduction to Leonhardi Euleri opera omnia vol X et XI seriei secundae. Leonhardi Euleri opera omnia. Series 2, Opera mechanica et astronomica. 1960, Turici: Orell F©∗ssli. p. 435.
Wang, C.Y., 1981. Large deflections of an inclined cantilever with an end load. Int. J. Non Linear Mech. 16 (2), 155–164.
Wang, J., Chen, J.K., Liao, S.J., 2008. An explicit solution of the large deformation of a cantilever beam under point load at the free tip. J. Comput. Appl. Math. 212 (2), 320–330.
Wang, Y.G., Lin, W.H., Liu, N., 2012. A homotopy perturbation-based method for large deflection of a cantilever beam under a terminal follower force. Int. J. Comput. Methods Eng. Sci. Mech. 13 (2), 197–201.
Whittaker, E.T., Watson, G.N., 1927. A Course of Modern Analysis: An Introduction to the General Theory of Infinite Processes and of Analytic Functions, with An Account of the Principal Transcendental Functions, fourth ed. Cambridge University Press, Cambridge, p. 608.
Yau, J.D., 2010. Closed-form solutions of large deflection for a guyed cantilever column pulled by an inclination cable. J. Mar. Sci. Technol. Taiwan 18 (1), 130–136.
Zakharov, Y.V., Okhotkin, K.G., 2002. Nonlinear bending of thin elastic rods. J. Appl. Mech. Tech. Phys. 43 (5), 739–744.
Zakharov, Y.V., Zakharenko, A.A., 1999. Dynamic instability in the nonlinear problem of a cantilever. Vychysl. Tekhnol. (in Russian) 4 (1), 48–54.
Zakharov, Y.V., Okhotkin, K.G., Skorobogatov, A.D., 2004. Bending of bars under a follower load. J. Appl. Mech. Tech. Phys. 45 (5), 756–763.
Zhang, S., Jin, J., 1996. Computation of Special Functions, vol. 26. Wiley, New York, Chichester, p. 717.